Stereophotographic Measurement of Joint and Bedding Orientation at Thornton Quarry, Illinois

Christopher J. Stohr, Justine Petras, Donald G. Mikulic,
and Jason Thomason

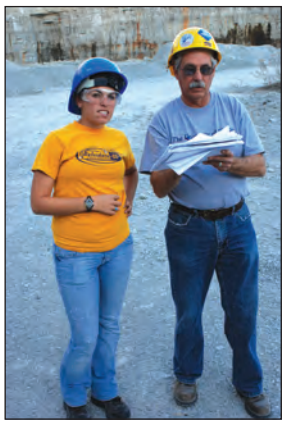

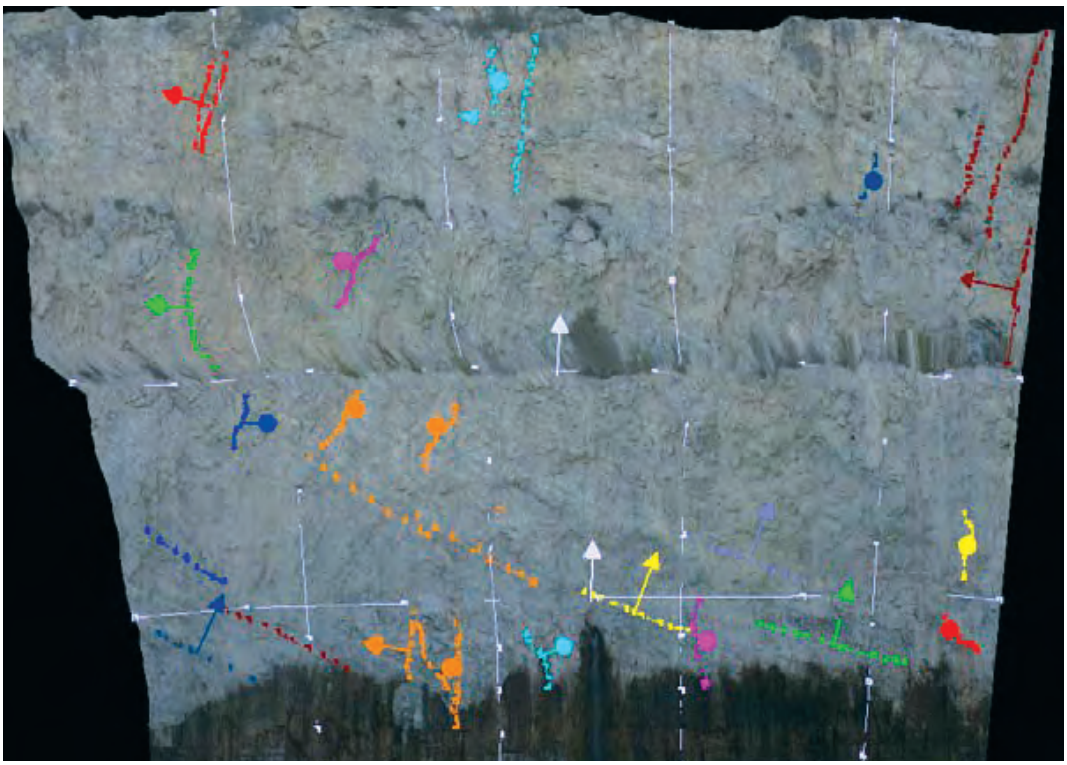

Circular 579 2011

ILLINOIS STATE
GEOLOGICAL SURVEY
PRAIRIE RESEARCH INSTITUTE

ILLINOIS STATE GEOLOGICAL SURVEY
Prairie Research Institute
University of Illinois at Urbana-Champaign

Front Cover: *(a) Justine Petras and Christopher J. Stohr in Thornton Quarry. (b) Joints, fractures, and bedding continuity segments digitized on a stereomodel. (c) Donald G. Mikulic in Thornton Quarry.*

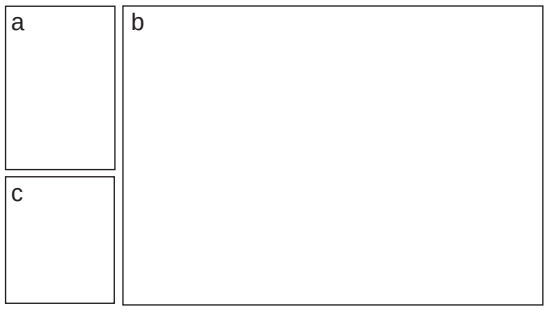

© 2011 University of Illinois Board of Trustees. All rights reserved.
For permissions information, contact the Illinois State Geological Survey.

Stereophotographic Measurement of Joint and Bedding Orientation at Thornton Quarry, Illinois

Christopher J. Stohr, Justine Petras, Donald G. Mikulic, and Jason Thomason

Circular 579 2011

ILLINOIS STATE GEOLOGICAL SURVEY
Prairie Research Institute
University of Illinois at Urbana-Champaign
615 E. Peabody Drive
Champaign, Illinois 61820-6964
http://www.isgs.illinois.edu

CONTENTS

Figures

Tables

Background

The dolomite excavated from the Hanson Materials Service quarry at Thornton, Illinois, has been used for construction materials and related purposes in the Chicago metropolitan region since the mid-1800s. Because of the extensive exposures created by more than 150 years of quarrying, Thornton reef is one of the best exposed ancient reefs in North America. The exposure is so well-known among geologists and earth scientists that the quarry is known to them simply as "Thornton." The excavation itself has grown so large that it has become a prominent landmark (Figure 1).

Rock excavated at the quarry is from a Silurian-age reef formed about 430 million years ago when the Chicago area was located 20 degrees south of the equator. The early stages of reef development produced a steeply sloping core in the form of a roughly northwest-southeast–trending ridge. Most of the reef was built by the cyclic deposition and cementation of sediment derived from the remains of calcareous marine plants and animals. These processes are represented by steeply dipping beds that appear as alternating light and dark bands (Lowenstam 1952, Mikulic and Kluessendorf 1999). The extant reef structure is 1.5 miles in diameter and at least 350 feet thick.

The exposed rock at Thornton gives an unusually detailed glimpse into the development of ancient reefs of the central United States, particularly the Silurian-age reefs that occur throughout the Illinois Basin (Figure 2). Silurian reefs are an important source of high-quality construction aggregate in the northern part of the state where they occur in areas of thin overburden. In the southern part of the state in the deeper portions of the Illinois Basin, the reefs are petroleum reservoirs occurring several hundred feet in the subsurface. These reservoirs may be used as gas storage reservoirs for natural gas supplies or for the geological sequestration of carbon dioxide (Whitaker 1988, Benson 2005).

Recently, the Metropolitan Water Reclamation District of Greater Chicago (MWRDGC) has begun using part of the quarry as a storm water reservoir with a capacity of 3.1 billion gallons (Figure 3). Floodwater is diverted from Thorn Creek and the Little Calumet River through a tunnel to the lower west lobe of the quarry for retention until released through the Calumet Water Reclamation District Plant and discharge into the local waterways. The north lobe will become the composite reservoir when excavation is completed, and it will replace the transitional reservoir in the lower west lobe, which will be returned to quarry operations.

Using parts of the quarry for storm water retention temporarily covers significant parts of the reef. Study of the important areas in the lowest part of the quarry is already somewhat restricted because of inaccessibility and safety considerations. More important, however, are the active mining operations at the site, which constantly remove and change exposures. For example, quarry operators have in recent years discussed removing the single most important exposure, which demonstrates how the reef initially developed. Because the strata exposed at Thornton quarry are an important reference for teaching and research, a method for recording the stratigraphy and structure of the exposure in three dimensions is desirable.

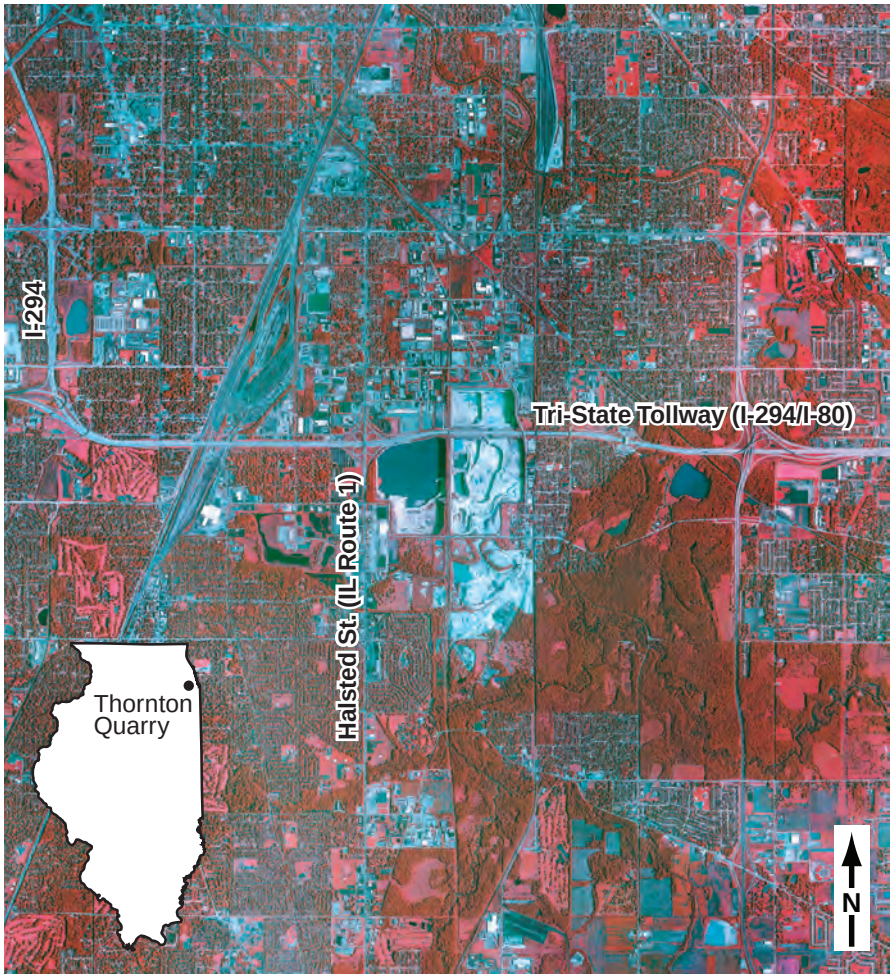

Figure 1 The 1.5-mile-diameter Thornton quarry in the center of this color infrared orthophotograph exposes a Silurian-age reef in metropolitan Chicago. A railroad easement separates the main and lower west lobes. Vegetation appears red; the dolomitic rock appears blue-white. (Imagery is from the 2010 National Agricultural Imagery Program.)

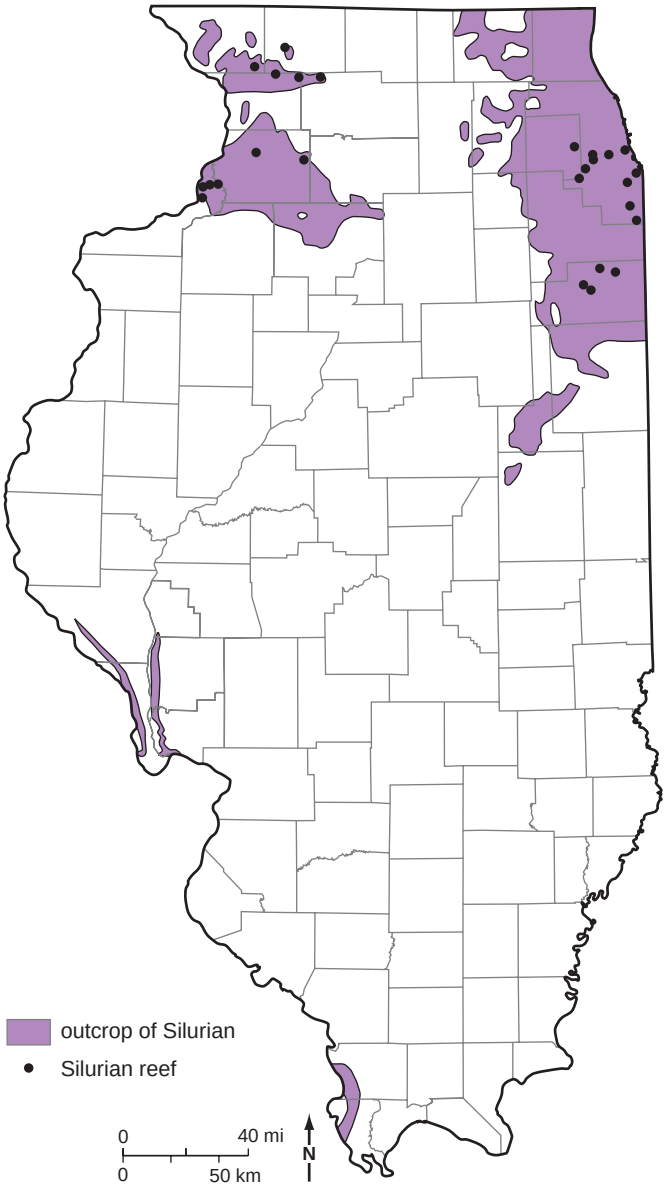

Figure 2 Distribution of Silurian rock and reefs at the bedrock surface in Illinois.

Several remote methods are used to make three-dimensional (3-D) measurements at inaccessible locations: surveying using a reflectorless total station (Stohr et al. 2008), terrestrial LIDAR scanning (Bellian et al. 2005), and close-range photogrammetry (Alfarhan et al. 2008, Haneberg 2008). Close-range photogrammetry using uncalibrated high-resolution digital cameras is a relatively low-cost method for acquiring the imagery used to make a georeferenced stereomodel of an outcrop. The high-resolution photography permits the recording of subtle features such as bedding characteristics, small conduit openings, and closed joints.

Stereophotogrammetry (making measurements using stereophotography) is similar to making topographic maps by aerial photogrammetry methods. Photogrammetry is referred to as close range because the object photographed is typically closer than aircraft altitudes of thousands of feet. Close-range photogrammetry is an old method being newly applied for collecting, measuring, and documenting geologic data. By matching pixels on the photographs composing the stereopair, a digital elevation model (DEM) is constructed. The DEM points are connected to create a surface model from which information about the geometry of features in the soil and rock can be measured. Measurements such as inclination of a surface including dip and dip direction, openings, and thickness can be calculated, and vertical and horizontal changes in bedding, lithologic contacts, and other interpretations can be geographically referenced for 3-D modeling.

Close-range photogrammetry provides the capability to measure joint properties such as dip and direction, lengths, spacing between joints, and vertical and lateral changes in material properties as georeferenced measurements for improving mine safety, extraction, and subsequent use. This capability is a great advantage for inaccessible or dangerous locations, such as at active quarry operations.

Description of Outcrop Close-Range Photogrammetry

Stereophotogrammetry of geologic outcrops includes collecting a pair (or more) of photographs of an exposure, surveying control points on the outcrop and camera stations, and processing to measure fracture and joint face orientation, dip, and dip direction (Figures 4, 5, and 6). This method has been used primarily for stability analysis of rock slopes along highways and surface mines (Haneberg 2008). The method consists of two operational phases: field data collection and office data processing and analysis.

Field data collection includes these steps:

- Survey reference (control) stations using global positioning system (GPS) technology.
- Collect stereophotography of the quarry walls.
- Survey each camera station and control points located on the quarry wall using reflectorless total station.

Figure 3 A color orthophotograph showing study sites at the reef apex and north flank of the main lobe. (Imagery is from the 2010 National Agricultural Imagery Program.) Study sites are shown in detail in Figures 7 and 8.

- Sketch and identify control on field mosaicked photography.

Office processing and analysis are as follows:

- Process global positioning system (GPS) and total station control data to local coordinates.
- Convert raw digital photographs to .tif image file format.
- Develop a stereomodel and derive a DEM using specialty software.
- Digitize joints, polygon surfaces, bed contacts, and features of interest on the georeferenced stereomodel.
- Conduct statistical analysis of joint, dip, dip direction, and other data.
- Export data to Geographic Information Systems (GIS) or other software for display (optional).

Details of the close-range photogrammetry procedures are described in Appendix 1. All of the close-range photogrammetry, stereomodel generation, and feature digitizing were performed using Sirovision® and Sirojoint® software version 3.3. Leica GeoOffice version 6 was used to process survey data.

Advantages of photogrammetry are reduced equipment cost, fast processing, and integration of high resolution photographs with the underlying DEM extracted by the software. Disadvantages include the need to make several stereomodels along a section, depending on the proximity to the target section. Proximity can also restrict the angle viewed. Even a small, undocumented misorientation of camera along a section can complicate processing and adversely influence the accuracy of the stereomodels. We found that the overall accuracy of the stereomodels derived by close-range photogrammetry is acceptable for most geologic work.

Figure 4 Collecting stereophotography at the reef apex.

Study Sites

For this study, stereophotograph images were collected at two sites, one at the reef center (reef apex, Figure 3) on November 3 and 4, 2008, and the other at a north-south wall exposing a northern flank of the reef (north flank, Figure 3) on November 4, 2008. Our investigation was concentrated on the north flank site.

Data at the reef center were collected along a haul road adjacent to the quarry wall. The distance from a camera station to the outcrop wall was about 140 feet; the distance between camera stations was 20 feet. There were 48 camera stations at this site: 24 level and 24 tilted. Twenty-six ground control points were collected at the site (Figure 7). Several of the possible stereomodels were made; however, all exhibited large errors because of camera misorientation (optical axis was not aligned parallel or slightly convergent), and the oblique photographs were not corrected for tilt.

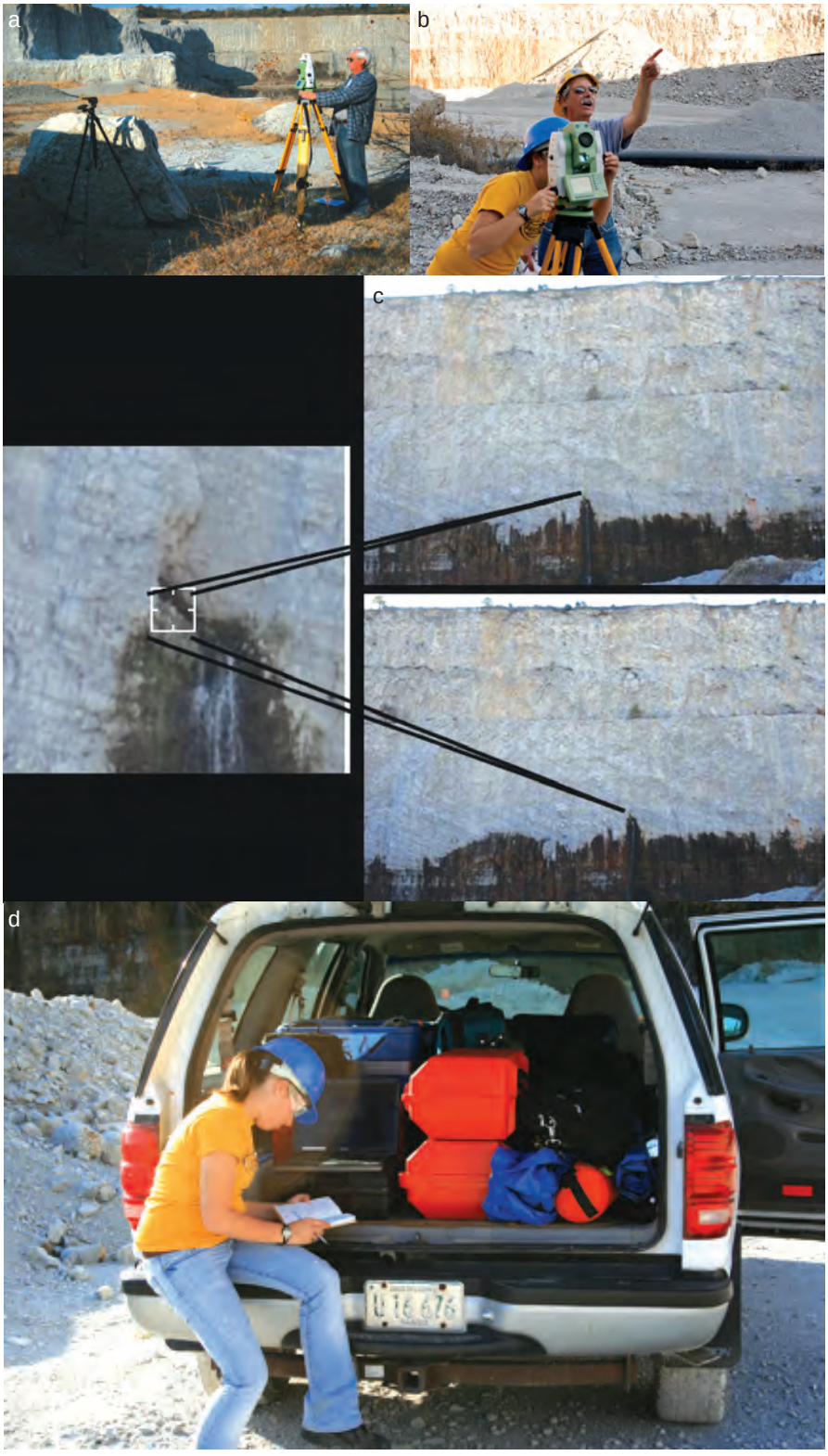

Figure 5 Surveying the camera station (a) and the reference mark on quarry wall (b and c) and noting the mark location on the photomosaic on a notebook computer (d).

Data at the north flank site were collected in a nearly ideal setting for close-range photogrammetry: an unused haul road parallel to the 300-foot-high quarry wall (Figure 8). The minimum distance from camera station to the outcrop wall was 580 feet, which allowed the entire vertical section of the quarry wall to be photographed with a pixel resolution of 0.11 feet. Separation between the seven camera stations was nominally 75 feet, allowing 900-foot section of the wall to be photographed. Twenty-one ground control points were collected along the north-south wall, including some outside the 700-foot-long section where stereomodels were extracted. Deep, steeply sloped, water-filled excavations were adjacent to most of the section.

Results and Discussion

Joint Spacing

Occurrence, length, spacing, and orientation of discontinuities are important considerations in modeling slope stability and rockfalls, fluid movement, and quarrying (Terzaghi 1965). Joints, fractures, and bedding are the types of discontinuities studied here. Because joints and fractures were indistinguishable on the stereomodels, they are analyzed together and termed joints for purposes of discussion. Joints and fractures are differentiated according to orientation in a later section.

Spacing is the shortest lateral distance between joints as measured on stereomodels. Only the joints to the immediate right or left of the joint of interest were measured for joint spacing. A compilation of some of the joints and bedding continuity measured at the north flank site is shown in Figure 9. Joints measured from individual stereopairs are shown in Appendices 2 through 7.

Spacing between the same joint pairs measured on multiple stereomodels appears to be consistent (Table 1). For example, one joint pair spacing is 5.8 feet for joints 19 and 18 (stereomodel 3008-3009), 5.7 feet for 12 and 8 (3009-3010), 5.7 feet for 7 and 8 (3010-3011), and 5.6 for 7 and 8 (3011-3012). The average measured difference in the spacing between the same joints on

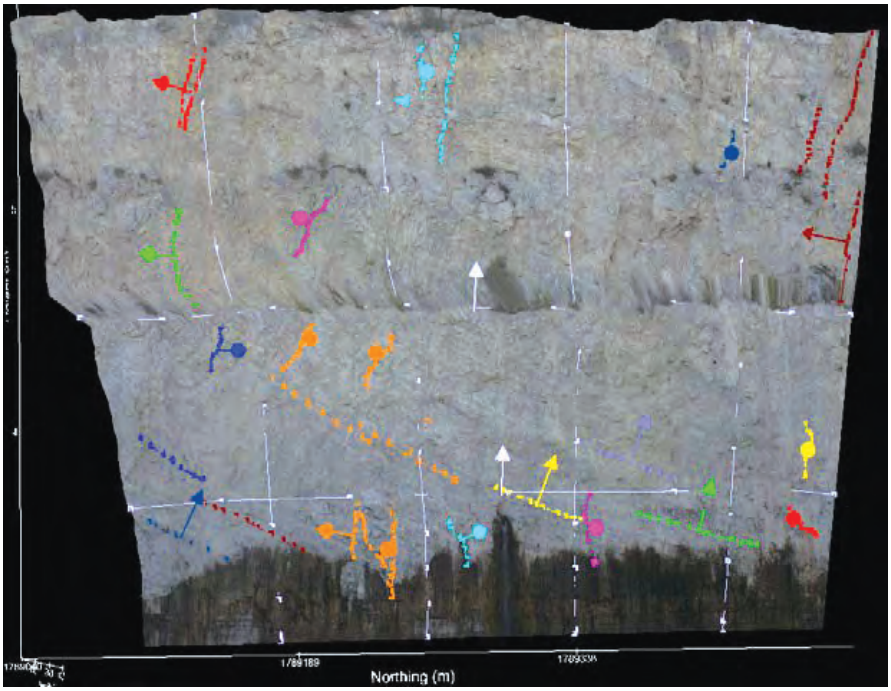

Figure 6 Joints, fractures, and bedding continuity segments digitized on a stereomodel.

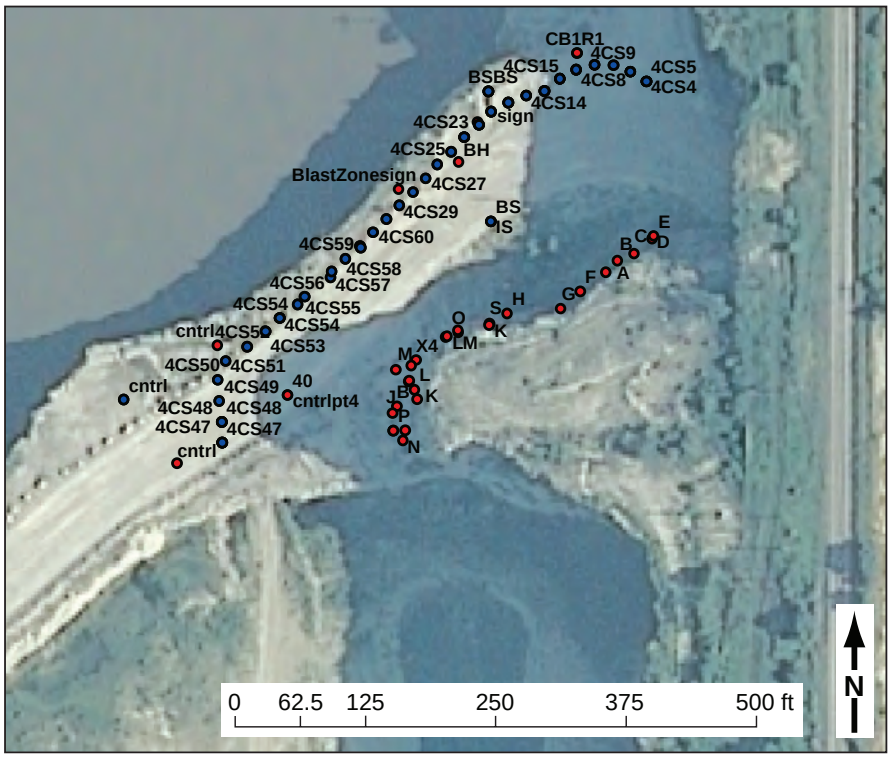

Figure 7 A 2005 color orthophotograph of the Chicago Urban Area showing 48 camera stations (blue) and 26 ground control points (red) surveyed near the apex of the reef. Quarry location is shown on Figure 3.

different stereomodels is 0.3 feet; for image pairs 3009-3010 and 3010-3011, the numbers are identical. The worst of the measured pairs is joints 3 and 4 (3007-3008) and joints 5 and 6 (3008-3009), which differed by 6 feet. Two other joint pairs differed by 0.4 and 1 foot between stereopairs. The high degree of agreement demonstrates consistency of relative measurements between stereomodels.

Distance between the joints ranges from 6 to 250 feet. The average spacing of joints in all stereomodels of the north flank is 71 feet, although the trend appears to have a log-normal distribution with multiple deviations and gaps (Table 1 and Figure 10). Comparison of joint spacing (Figure 10) with joint length (Figure 11) shows that short joints tend to be closely spaced, and long joints are more distantly spaced. This distribution suggests that there are multiple causes of joint formation from natural forces such as regional stress and fracturing caused by quarrying activities.

Joint Length, Magnitude, and Orientation

The outcrop at the north flank study site is a nearly vertical wall oriented north-south; consequently, measurements for the 44 joints studied in this section are not truly representative of the magnitude and orientation of all joint sets within the quarry. The lack of polygonal planar surfaces on which to measure dips and strikes of the closed joints on the stereomodel in Sirovision caused us to use a less desirable method for measurement by digitizing the fracture traces along a single face of a joint. The inclinations presented ordinarily would be considered apparent dips; i.e., inclinations that are not perpendicular to the strike or true dip and are of lesser magnitude than true dips. However, comparison of the dips recorded by others using traditional methods, results of statistical analyses, and discussion with experienced professionals about the methodology indicates that the measurements are comparable with true dips. At least some of the variation observed in the measurements might be caused by polygonal fracturing during formation

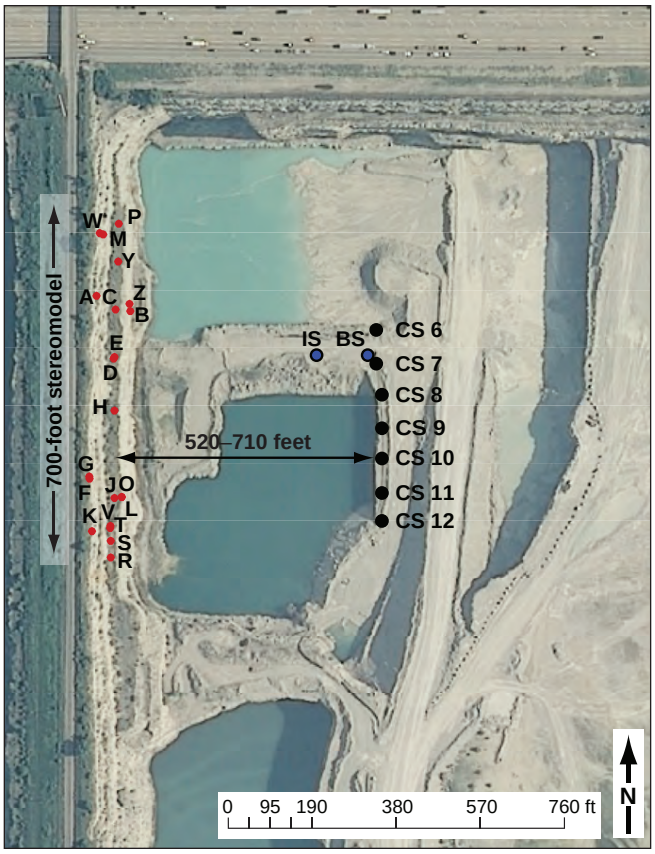

Figure 8 Twenty-one ground control points (letters) surveyed at a 300-foot-high exposure on the north flank of the reef (quarry location on Figure 3). Photography was collected at 7 camera stations (numbered 6 through 12) along a short haul road to create a 700-foot stereomodel for this study. (Imagery is from the 2010 National Agricultural Imagery Program.)

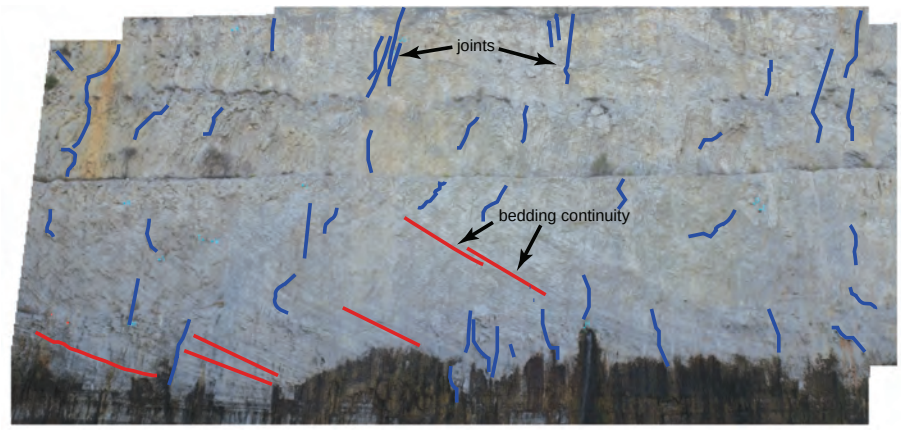

Figure 9 Compilation of joints (blue) plotted on a mosaic of orthorectified imagery of the north flank study site. A partial compilation of bedding continuity measurements are shown in red.

and subsequent deformation of the reef (Laufeld et al. 1978).

Most joints are between 20 and 40 feet in length and average about 36 feet (Figure 11 and Table 2). Lengths are considered to be accurate within the range of error described later in the error of control section. Seven joints are longer than 50 feet, and only a single joint was longer than 100 feet. None extended the entire 300-foot-high quarry wall. Longer joints are more nearly vertical. Short joints might be a consequence of blasting or quarrying activity or polygonal fracturing and deformation. Some of the joints measured are shown in Figures 6 and 9.

There is little variability in dip magnitude of the joints; all but a few are greater than 70 degrees (Figure 12a). The deviants may be an artifact of a joint oriented at an acute angle to the wall. The nearly vertical orientation of most joints is consistent with regional trends (Foote 1982).

The presence of three centroids of joint dip direction (Table 2 and Figures 12a and 13) were confirmed by the k-means clustering analysis (Figure 12b). Clustering is an iterative process that agglomerates data into a specified number of groups according to the distance to the arithmetic mean (centroid). The process of computing centroids is repeated until convergence when points are not reassigned to other clusters. Joint data from each stereomodel are reproduced in Appendices 2 through 7.

Interpretation of joint orientation of a single vertical wall can be problematic where calculations of orientation and magnitude of dip slopes are based upon point coordinates digitized along a joint trace rather than a plane surface. However, analysis of the joint data for the north flank site demonstrates that our measurements, which are based upon traces, can be treated as planes and analyzed by eigenanalysis.

For this study, eigenanalysis, a statistical method for analyzing vector data, was used to determine the predominant orientation and degree of alignment of dips and strikes, which can be quantified by calculating the first eigenvector and associated eigenvalue,

Table 1 Joint spacing measured in stereomodels at the north flank site.[1]

Image pair	Joints	Spacing (feet)	Image pair	Joints	Spacing (feet)
3006-3007	1 and 3★	47.3	3008-3009	12 and 11	18.9
	3 and 4	68.2		14 and 12	11.8
	4 and 12	59.6		15 and 13	154.0
	12 and 5	66.1		13 and 14	42.5
	6 and 2	237.3		16 and 15	14.7
	7 and 8	16.6		18 and 16	121.5
	8 and 9	34.3		20 and 17	71.1
	7 and 10	49.7		19 and 18■	5.8
	10 and 11	30.9	3009-3010	1 and 2	120.9
3007-3008	1 and 2	18.3		2 and 3	104.6
	2 and 5	56.9		3 and 4	6.1
	3 and 4•	45.6		4 and 5	15.9
	4 and 7	130.3		6 and 7	110.2
	5 and 6★	48.3		7 and 10	249.3
	6 and 8	73.9		8 and 9	136.6
	8 and 11	39.4		9 and 11	153.3
	9 and 10	51.4		12 and 8■	5.7
	10 and 12	41.1	3010-3011	1 and 2	115.4
	12 and 13	12.7		3 and 4	32.7
3008-3009	1 and 2	11.3		5 and 6▲	105.0
	2 and 3	16.1		7 and 8■	5.7
	3 and 7	33.2		8 and 9	133.2
	4 and 5	45.8	3011-3012	1 and 2	205.2
	5 and 6•	39.6		3 and 4	69.4
	6 and 10	234.2		5 and 6	43.9
	7 and 8	68.3		6 and 9▲	105.4
	8 and 9	116.0		7 and 8■	5.6
Mean		71.4			
Standard deviation		62.5			
Maximum		249.3			
Minimum		5.6			

[1]Joint pairs are not numbered consistently between image pairs; however, symbols indicate pairs occurring on several stereopairs.

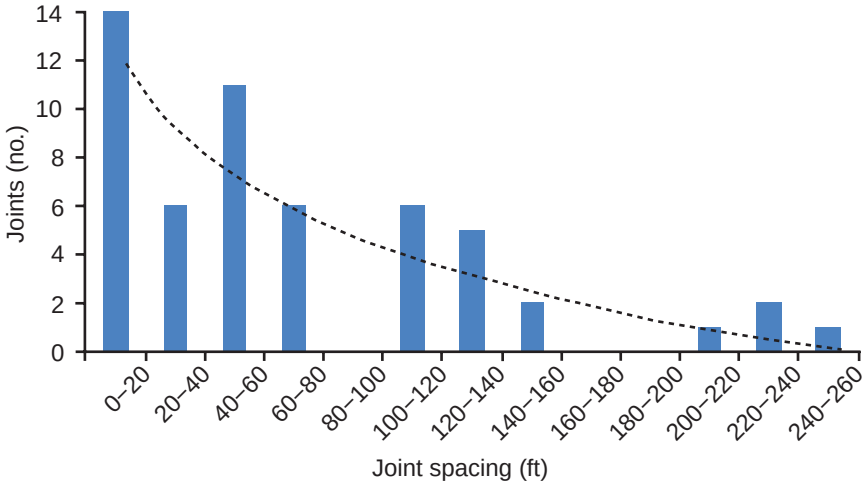

Figure 10 Joint spacing at the north flank study site. The logarithmic trend has been fitted to the data.

respectively. Table 3 displays poles of joint faces as vector measurements (dip and dip direction) (Davis 2002).

The E1 eigenvector corresponds to the orientation of the dominant direction of dip of a joint set (Scheidegger 1965, Friedman and Weisberg 1981, Marcotte and Henry 2002).

Table 3 shows normalized eigenvalues for the three joint set clusters shown in Figure 12. Eigenvalues are normalized between 0.33 (random) and 1.0 (perfectly aligned). The maximum eigenvalue (Table 3) for each of the clusters is relatively high (>0.85) (Scheidegger 1965). Thus, the confidence of predicting joint orientations is relatively good, and the orientations are consistent with prior studies at the site. This demonstrates reliability in the photogrammetric measurements of dip and the dip direction.

E1 eigenvectors of the three joint sets (Table 3) translated into strikes and dips (normal to the eigenvectors) in Table 4 are similar to previous measurements in other studies. A discontinuity roughly aligned with the north-south wall is probably a fracture set developed as result of quarry activities and blasting, which has not been discussed in those previous studies.

Bedding Thickness and Continuity

Two lithologic formations are seen within the stereomodels; both are dolomitic reef rocks of Silurian age. The Racine Dolomite (Niagaran Series) unconformably overlies the older Sugar Run/Joliet Dolomite (Mikulic and Kluessendorf 1999). Joints and bedding in the lower units are difficult to see because water stains and rock piles obscure part of the wall (Figures 6, 9, 14, and 15). Only those joints within the Racine Dolomite were digitized.

Eroded from higher elevations near the center of the reef, bioclastic debris layers settle along the reef flanks. Individual flank beds occur as thin, cyclic, light-and-dark couplets in which the bioclastic debris fines upward (Donald G. Mikulic, personal communication, 2009). The difference in materials is

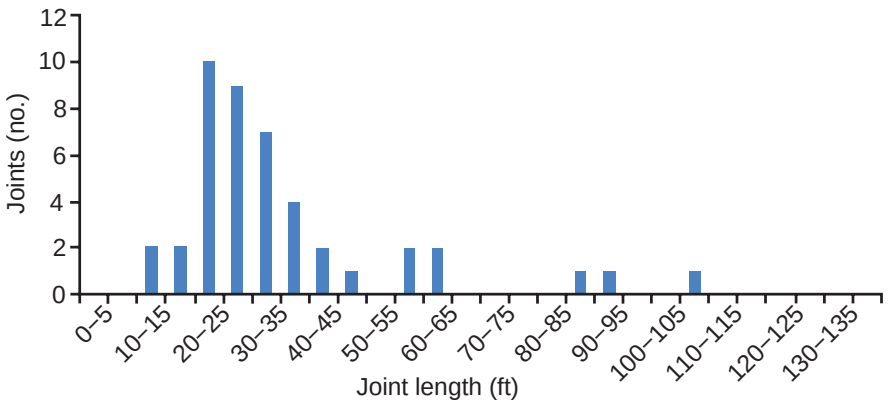

Figure 11 Length of joints at the north flank study site.

Table 2 Summary of joint length, dip magnitude (degrees), and dip direction (DDN) (degrees) at the north flank site.

Stereomodel	Joint	Dip	DDN	Length (feet)	Stereomodel	Joint	Dip	DDN	Length (feet)
3006-3007	1	82.2	83.9	21.7	3008-3009	2	77.3	304.6	30.5
	2	72.6	139.6	22.3		4	62.4	143.5	23.0
	3	81.5	86.8	38.5		7	73.0	65.0	26.2
	4	62.3	31.4	22.1		10	85.0	101.3	28.8
	5	57.6	88.4	14.4		11	76.4	185.5	89.9
	6	67.1	128.7	21.2		12	74.4	198.7	94.0
	7	83.4	230.8	17.7		15	79.8	176.1	60.2
	8	82.1	216.9	109.0		16	83.7	74.6	25.8
	9	75.9	139.8	34.0		17	70.0	125.1	36.0
	10	70.4	197.6	33.3		18	74.1	171.4	35.5
	11	69.8	174.3	56.2		19	80.3	218.1	32.3
	12	57.6	88.4	14.4		20	81.6	134.8	48.3
3007-3008	1	80.1	136.4	27.8	3009-3010	1	78.5	86.0	59.3
	2	85.8	103.5	40.2		6	77.8	247.3	26.7
	3	61.8	105.4	30.7	3010-3011	1	82.9	61.2	31.5
	4	72.4	103.2	27.0		2	80.4	142.3	24.7
	7	70.7	257.4	23.8		3	78.3	38.8	26.0
	8	83.3	311.6	18.1		5	74.1	133.6	26.4
	9	44.2	140.9	27.1	3011-3012	1	83.4	133.7	41.9
	10	74.5	195.3	20.8		3	80.1	51.3	23.8
	11	64.1	102.7	23.1		5	56.4	143.6	38.3
	12	74.5	221.3	35.0					
	13	83.5	221.7	63.1					
Mean		74.2	146.4	35.7					
Standard deviation		9.2	67.6	20.7					
Maximum		85.8	311.6	109.0					
Minimum		44.2	31.4	14.4					

likely due to differences in hydraulic and other geotechnical properties.

Cyclicity is less conspicuous near the reef center, becoming more pronounced in the distal flanks. Figure 14 shows a light layer decreasing in thickness as the strata overlie a dark layer. Immediately below that layer is an example of tapering beds where a light layer appears to pinch out completely, a lateral discontinuity. As the flank bed couplets vary in thickness, composition, and continuity, discontinuous changes in lateral and vertical porosity can be expected.

Couplets of light and dark beds vary in length from 20 to nearly 115 feet (Table 5). Individual beds range in thickness from 0.4 to 1.2 feet, but beds are likely to be thicker or thinner. Thicker beds may be couplets in which the light or dark layers are too thin to be discernible in the images.

Dip of the beds is steepest at the apex, 41 degrees, and decreases to nearly flat-lying. Vertical jointing in the two directions shown in Table 4 crosscut the beds, which likely permits free movement of fluids.

Bedding Orientation

The apparent direction of the inclination of the bedding planes is to the north-northeast, away from the center of the reef. Table 5 summarizes the bedding plane data. Individual bedding plane data for each stereomodel are in Appendices 2 through 7. Bedding plane dips range from 41 degrees to nearly horizontal; inclination decreases as distance from the reef apex increases.

Water Seepage

Water seepage can be seen clearly in specific portions and points of the quarry wall. Most water evidence is from staining and algal growth at the lower portion of the exposure. There is a single point where water flow is continuous (Figure 15). The uppermost water seepage is observed at the contact between the Racine Dolomite and underlying Sugar Run/Joliet Dolomite.

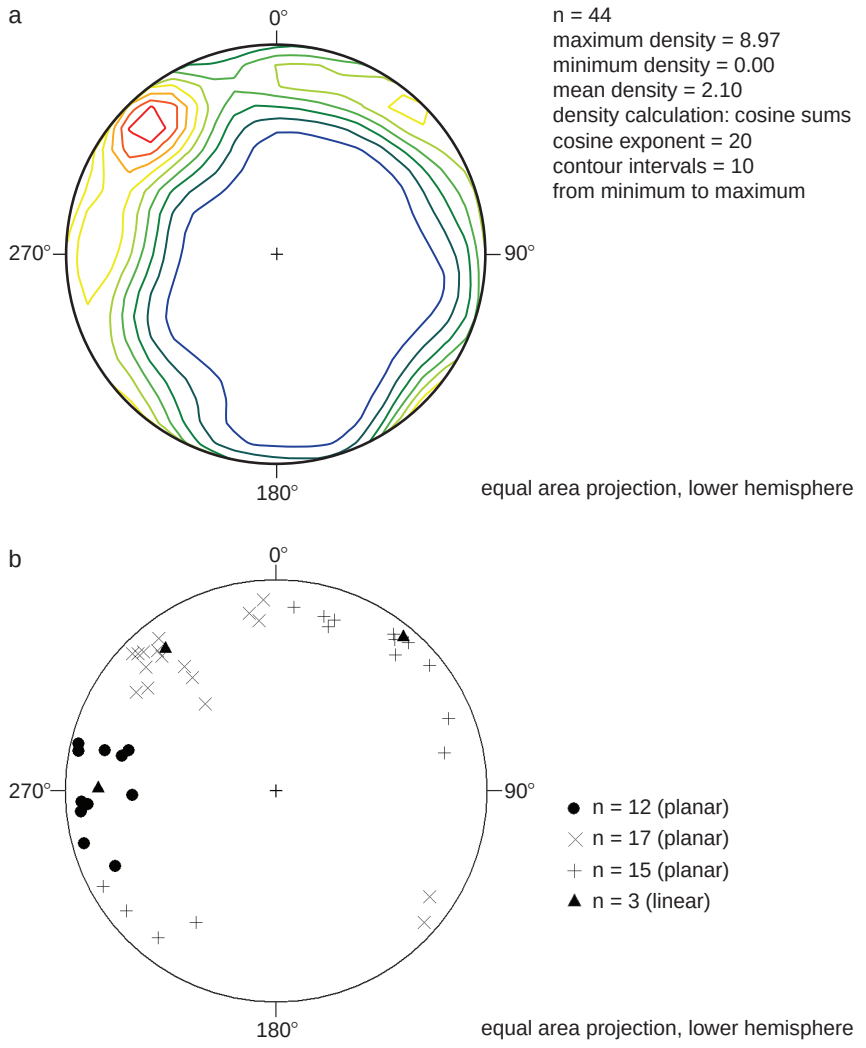

Figure 12 Stereogram of joint dips at the north flank site density contoured (a) and aggregated into three clusters by the k-means algorithm (b) (Stereo32, version 1.0.2.). The equal area stereogram (b) includes the three cluster means, increasing the total number of joints plotted.

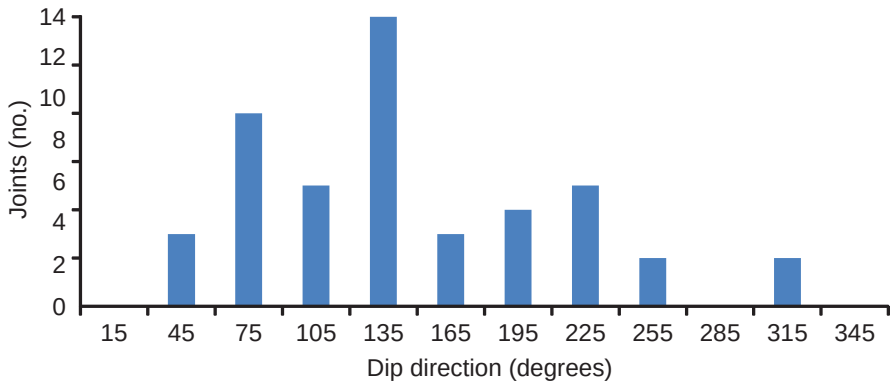

Figure 13 Histogram of joints and dip direction at the north flank site.

Conduits and Openings

There are 16 conduit openings found in the study site wall (Table 6). Openings average 2 feet in diameter. The smallest is 0.9 foot, and the largest, at 6.7 feet in diameter, is control point E, the prominent orifice of a waterfall (Figure 15). Spatially, the conduits and openings appear to occur more frequently toward the south side of the wall nearer the apex of the reef. Conduit data are listed in Table 6.

Control and Check Point Error

Control points are well-known absolute positions used in surveying and photogrammetry for georeferencing a total station or creating photogrammetric stereomodels used for making measurements. Check points are well-known positions not used for computing a stereomodel but for comparing the measurements to independently determine the accuracy of the model.

Error is endemic to all types of measurement. Absolute error is the difference between the exact (absolute) position and its approximation in a model. Relative error is the difference in distance between positions in a model compared with the distance between control or check points.

When a stereomodel is created, errors are distributed among all control points, changing their original values to new calculated positions. Table 7 shows the displacement of the control points for the stereomodels. The control points for this study are not well-known for several reasons: (1) the control points used for the total station were determined by independent GPS surveys and were not adjusted within a local or regional network; (2) the control points used for the stereomodels were surveyed by unbalanced foresight/backsights because of site and time limitations; and (3) the natural targets (cracks, prominent point) used for the stereomodel control points are ambiguous.

Tables of error for control and check points used for the individual stereomodels are found in Appendices 2 through 7. The error represented in

Table 3 Eigenvectors and normalized (N.) eigenvalues of three clusters of 44 joints at the north flank site.

Cluster		E1	E2	E3
1	N. Eigenvalue	0.8505	0.1001	0.0494
	Azimuth	39.55	308.25	156.89
	Plunge	6.20	11.73	76.69
2	N. Eigenvalue	0.8861	0.0733	0.0406
	Azimuth	321.55	61.48	208.57
	Plunge	15.81	31.33	54.05
3	N. Eigenvalue	0.9278	0.042	0.0302
	Azimuth	270.79	7.46	145.51
	Plunge	16.72	21.15	62.52

those tables is the 3-D linear difference between surveyed and photogrammetry-derived coordinates for the same point. Sirovision uses a single control point identified on the image and outcrop to establish georeferencing and three additional relative points to construct the stereomodel.

Table 7 is a summary of the errors comparing the surveyed points with control points in a stereomodel. The mean difference between the coordinates is 1.7 feet, a surprisingly large difference. However, when considered as relative errors, the absolute error divided by the minimum distance between the camera and outcrop, the discrepancy is less than the pixel size of 0.11 feet.

A comparison of locations in check points between surveyed values and coordinates from the 3-D model is presented in Table 8. Absolute errors exceed the few tenths of a foot found for instrument setup and backsight, although relative errors are within a pixel (0.11 feet).

Spacing values between a joint pair identified on four stereomodels were compared in order to estimate consistency of measurements between stereomodels (Table 9). The same points along the joints were used for all measurements. The spacing values are very consistent between stereomodels, i.e., standard deviation of 0.12 and 0.07 feet and statistically significant within the 95% confidence interval and within the 0.11-foot pixel resolution.

The larger than expected absolute error might be ascribed to two causes: (1) the unbalanced distance between the instrument and backsight prism (100 feet) compared with the longer distance between the instrument and control and check points on the quarry wall (580 to 630 feet) and (2) the ambiguity of physical features used for control and check points on the quarry wall. The first cause, and likely the principal source of error, was a result of inaccessibility and active use of haul roads at the time the control points were initially surveyed and because of the time constraints during the photogrammetric data gathering.

Because prisms cannot be attached or placed on the quarry wall for those same reasons, including restrictions on approaching the wall, physical features were surveyed for reference. The use of a physical feature introduces ambiguity in several ways, including averaging of the uneven surface illuminated by the laser, the varying diameter of the oval with distance and angle of the

Table 4 Strike of normal and high-angle joints at and around Thornton quarry as measured by several studies.

	Average strike of normal joints		
Study	Set I	Set II	Angle between joints
Foote 1982, east site	N49° E	N36° W	75–87
Djavid and Fitzpatrick 2008	N48° E	N46° W	92
Shuri and Kelsay 1984	N45° E	N45° W	90
Harza Engineering Company 1986	N42° E	N34° W	76
STS Consultants, Ltd.	N41.1° E	S44.5° E	85.6
	Eigenvector	Eigenvector	
This study, joint sets	N52.1° E	N50.4°W	102.5
This study, fracture	N0.30° E		

Table 5 Length and dip magnitude of bedding planes measured at the north flank site.

Stereopair	Name	Dip (degrees)	Length (feet)
3006-3007	bedding 1	24.9	41.1
	bedding 2	22.0	32.0
3007-3008	bedding 1	32.1	62.1
	bedding 2	24.3	74.7
	bedding 3	27.2	65.8
	bedding 4	37.4	39.8
3008-3009	bedding 1	25.6	48.5
	bedding 2	38.2	41.7
	bedding 3	33.7	58.2
	bedding 4	39.8	62.1
	bedding 5	32.1	59.2
	bedding 6	21.7	50.8
	bedding 7	22.6	55.6
	bedding 8	15.5	66.7
3009-3010	bedding 1	16.7	30.8
	bedding 2	4.2	38.0
	bedding 3	18.2	43.5
	bedding 4	21.3	62.5
	bedding 5	28.4	22.0
	bedding 6	28.2	66.0
	bedding 7	32.3	69.2
	bedding 8	1.6	22.4
	bedding 9	41.2	20.1
3010-3011	bedding 1	6.2	114.7
	bedding 2	17.7	52.0
	bedding 3	23.9	58.6
	bedding 4	28.1	95.6
	bedding 5	3.0	69.2
	bedding 6	25.6	54.7
3011-3012	bedding 1	22.3	89.4
	bedding 2	40.2	85.5
	bedding 3	20.6	45.6
	bedding 4	33.2	47.1
	Mean		55.9
	Standard deviation		21.2
	Maximum	41.2	114.7
	Minimum	1.6	20.1

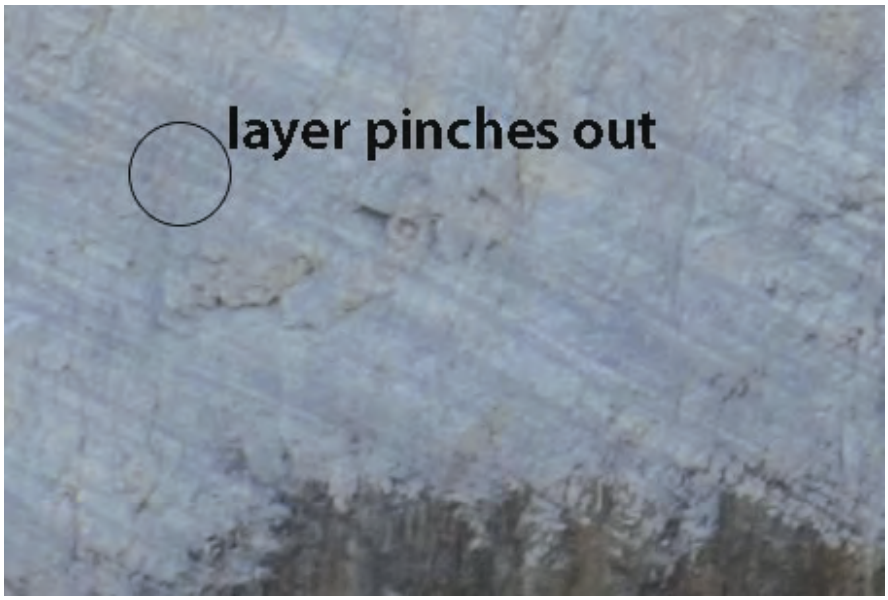

Figure 14 Change in bedding thickness and continuity at the north flank site. Circle shows where a light-toned bed exhibits pronounced change in thickness. The light-toned bed pinches out completely. Note the dark algae and stains from groundwater on the lower edge.

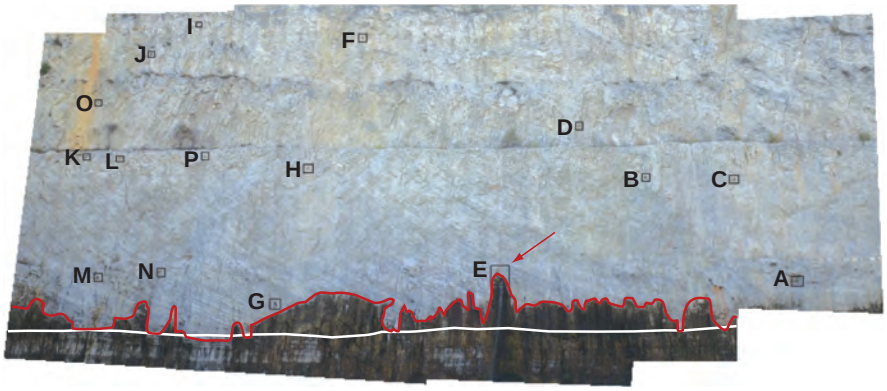

Figure 15 The stratigraphic boundary between the Racine Dolomite and the Sugar Run/Joliet Dolomite is marked by a white line on mosaic of orthorectified imagery. A red line marks the stains and algal growth from water flow near a stratigraphic boundary. An arrow marks the position of a waterfall issuing from a small conduit (control point E on Table 6).

laser beam to the irregular surface, and the uncertainty of identifying the surveyed object on the stereopair.

Although the absolute errors are larger than desired, the relative measurements (i.e., the comparison of joint spacing measurements between stereomodels) (Haneberg 2008) are within a pixel, 0.11 feet. Although there is error in absolute coordinates of surveyed and photogrammetric points, relative measurements between stereomodels are highly consistent.

Conclusions

Measurements of joint width, length, and spacing; location and dimensions of openings; and observations of bedding thickness and continuity in the reef structure in the Racine Dolomite were made on an inaccessible, 900-foot-long portion of a 300-foot-high, nearly vertical wall oriented north to south, exposing the north flank of Thornton reef (Figure 9). Close-range photogrammetry measurements were made using Sirovision software.

Our study found that nearly all joints are closed, were mostly vertical, averaged about 36 feet in length, and were spaced between 6 to 250 feet apart. Only one of the 44 measured joints was longer than 100 feet, and none extended the entire height of the wall.

Dips and dip directions measured as a trace along the nearly vertical joint faces were found to yield data equivalent to that of traditional measurements. Eigenanalysis of those measurements, which has never been conducted at the site prior to this study, offers a method of quantifying the predictability of joint orientations. The results of the eigenanalysis were consistent with results of previous studies at the site. Furthermore, eigenanalysis indicated a fracture set aligned parallel to the north-south wall, which is likely a consequence of mining operations.

Sixteen openings were identified. The largest opening, 6.7 feet in diameter, issues freely flowing water. It is located near the Racine Dolomite contact with the Sugar Run/Joliet Dolomite where staining and algae were observed on the bedrock.

Light-and-dark couplets of bioclastic debris in reef flank beds of the Racine Dolomite were found to be discontinuous; beds vary in length from 20 to about 114 feet. The thickness of individual beds range from 0.4 to 1.2 feet. Thick beds may contain multiple indistinct couplets. The dip of the beds is steepest at the center, 41 degrees, decreasing to nearly flat-lying. The lateral and vertical changes in beds likely result in changes in physical properties.

Physical and operational restrictions in setting control are a complication of any method that employs surveying and photography using fixed-focal length lenses. Error of absolute measurements in the stereomodels likely

Table 6 Conduit location and diameter at the north flank of the reef. Conduit E is the largest and only opening issuing flowing water. Coordinates in Illinois State Plane East Zone, NAD1983.

Conduit/ opening	Easting	Northing	Elevation (feet)	Diameter (feet)
A	1178329.4	1789505.4	351.7	2.5
B	1178293.7	1789402.5	435.8	2.6
C	1178297.3	1789469.9	431.9	3.0
D	1178259.7	1789353.4	489.7	1.9
E	1178303.0	1789282.8	361.0	6.7
F	1178237.5	1789150.8	586.8	1.4
G	1178310.0	1789109.1	337.4	2.0
H	1178297.0	1789126.2	444.5	1.1
I	1178250.2	1789010.2	593.0	1.0
J	1178256.6	1788970.1	564.4	2.0
K	1178290.0	1788934.8	457.3	1.2
L	1178289.6	1788964.2	455.3	0.9
M	1178302.6	1788964.2	354.3	2.5
N	1178305.1	1789014.5	362.2	2.7
O	1178263.6	1788929.9	513.8	1.6
P	1178291.6	1789036.0	458.3	2.2
Mean			449.8	2.2
Standard deviation			84.0	1.4
Maximum			593.0	6.7
Minimum			337.4	0.9

Table 7 Summary of error in location for control points used for stereomodels. Total absolute error is the linear distance between the values obtained through surveying and the digital 3-D model.

Image	Control point	Easting error (feet)	Northing error (feet)	Elevation error (feet)	Absolute error (feet)	Relative error (feet)
3006-3007	C	−0.75	0.07	0.32	0.82	0.001
3007-3008	E	1.68	0.13	0.04	1.68	0.003
3008-3009	H	−0.48	−1.20	1.59	2.05	0.004
3009-3010	H	−0.38	−1.10	2.53	2.78	0.005
3010-3011	G	1.11	−0.11	−0.26	1.15	0.002
3011-3012	J	−1.48	−0.03	−0.14	1.49	0.003
Mean		0.0	−0.4	0.7	1.7	0.003
Standard deviation		1.2	0.6	1.1	0.7	0.001
Maximum		1.7	0.1	2.5	2.8	0.005
Minimum		−1.5	−1.2	−0.3	0.8	0.001
t 0.975					0.797	0.0014

Table 8 Summary of error of 30 check points used for stereomodels. Total absolute error (feet) is the linear distance between the values obtained through surveying and the digital stereo model.

Image	Check points	Easting error	Northing error	Elevation error	Total error	Relative error
3006-3007	C	−0.75	0.07	0.32	0.82	0.001
	A	0.63	−1.33	0.48	1.55	0.003
	Z	−6.38	0.99	−0.27	6.46	0.011
	D	−1.99	1.84	−0.47	2.75	0.005
	E	−1.58	1.65	−0.44	2.32	0.004
	H	0.22	3.45	−1.06	3.61	0.006
3007-3008	D	1.47	0.29	0.10	1.50	0.003
	H	6.45	1.34	3.23	7.33	0.013
3008-3009	D	−4.48	−2.45	1.83	5.42	0.009
	E	−3.93	−2.02	1.93	4.82	0.008
	F	−2.98	−0.15	0.93	3.13	0.005
	G	−3.11	1.58	−0.29	3.50	0.006
3009-3010	F	−4.31	5.08	9.98	12.00	0.021
	G	−2.67	−5.79	−11.63	13.26	0.023
	J	−5.70	−0.04	0.84	5.77	0.010
	V	−3.20	3.28	0.77	4.64	0.008
3010-3011	F	0.84	−2.33	0.77	2.60	0.004
	H	2.83	−3.08	3.28	5.31	0.009
	J	−1.21	−0.52	2.08	2.47	0.004
	K	1.81	2.55	−1.21	3.35	0.006
	S	−0.27	1.85	2.45	3.08	0.005
	T	−0.67	1.43	2.85	3.26	0.006
	V	−0.85	2.79	3.00	4.18	0.007
3011-3012	R	−0.08	8.02	−0.79	8.06	0.014
	F	1.62	−2.06	−2.44	3.58	0.006
	G	2.19	0.19	−3.63	4.24	0.007
	K	2.28	3.22	−4.55	6.02	0.010
	S	−1.62	2.28	0.14	2.80	0.005
	T	−1.10	1.92	0.61	2.30	0.004
	V	−1.65	4.06	0.51	4.41	0.008
Average		−0.9	0.9	0.3	4.5	0.0077
Standard deviation		2.8	2.7	3.4	2.8	0.0048
Maximum		6.4	8.0	10.0	13.3	0.0229
Minimum		−6.4	−5.8	−11.6	0.8	0.0014
t 0.975					30.8	0.0527

Table 9 Joint spacing for two pairs measured on several stereomodels.

Stereomodel	Joint spacing	Stereomodel	Joint spacing
3008-3009	5.84	3009-3010	5.67
3009-3010	5.67	3010-3011	5.67
3010-3011	5.67	3011-3012	5.55
3011-3012	5.55		
Mean	5.68		5.63
Standard deviation	0.12		0.07
t 0.975	±0.21		±0.10

stems from an unbalanced setup spacing between the instrument station and backsight, a consequence of site limitations at an active mine. Measurements of known locations have relatively high absolute errors — in excess of 1.7 feet; however, relative errors are within the dimensions of a pixel. Measurements such as joint dip and spacing are consistent among stereomodels.

Despite limitations, close-range photogrammetry permits recognition, interpretation, and reliable measurement of geologic features on imagery at inaccessible sites. The data are comparable with measurements made by others using traditional methods.

Acknowledgments

James Bastian, Toby Breedlove, and James Goldberg of Lehigh Hanson Heidelberg Cement Group helped the authors obtain access to the Thornton quarry during active operations. Kevin Fitzpatrick and Bipinbhai (Bipin) Patel of the Metropolitan Water Reclamation District of Greater Chicago and Mohammad Djavid of MWH Americas worked through their agencies on short notice to fund part of the field data acquisition at the quarry. Joseph Kissane and William Rochford of the U.S. Army Corps of Engineers-Chicago District provided copies of orthorectified photography of the quarry walls. Matt Schumacher, University of Waterloo, assisted in surveying and photographing the outcrops. James Best, Geology Department, University of Illinois at Urbana-Champaign, loaned GPS and reflectorless total station for the surveying. Xiaodong Miao consulted on statistical curve fitting. Several colleagues at the Illinois State Geological Survey contributed in expertise in editing, writing, and preparation for Web publication, especially Donald Keefer who suggested and obtained institutional support for the use of stereophotogrammetry for 3-D outcrop analysis. Carlos Aiken, University of Texas at Dallas, introduced the authors to the use of close-range photogrammetry and provided greatly appreciated advice. Stereo32 version 1.0.2 was provided by Klaus Röller and Claudia A. Trepmann. The manuscript was improved by the reviews of Bipinbhai (Bipin) Patel, Metropolitan Water Reclamation District of Greater Chicago; Wen-June Su, Illinois State Geological Survey; and William C. Haneberg, Haneberg Geoscience, Cincinnati, Ohio, who offered valuable suggestions.

References

AECOM Web site: http://www.cte.aecom.com/MarketsAndServices/39/39/index.html

Alfarhan, M., L. White, D. Tuck, and C. Aiken, 2008, Laser rangefinders and ArcGIS combined with three-dimensional photorealistic modeling for mapping outcrops in the slick hills, Oklahoma: Geosphere, v. 4, no. 3, p. 576–587.

Bellian, J.A., C. Kerans, and D.C. Jennette, 2005, Digital outcrop models: Applications of terrestrial scanning lidar technology in stratigraphic modeling: Journal of Sedimentary Research, v.75, no. 2, p. 166–176.

Benson, S., 2005, Chapter 5: Underground geological storage, *in* B. Metz, O. Davidson, H. De Conick, M. Loos, and L. Meyer, eds., Intergovernmental Panel on Climate Change Special Report on Carbon Dioxide Capture and Storage, Working Group III of the IPCC: Cambridge, United Kingdom and New York, Cambridge University Press, p. 195–276.

Davis, J.C., 2002, Statistics and data analysis in geology, 3rd ed.: New York, New York, John Wiley & Sons, 638 p.

Djavid, M., and K. Fitzpatrick, 2008, Connection of TARP tunnel to Thornton quarry reservoir: 9th North American Tunneling Conference, NAT 2008, p. 351–363.

Foote, G.R., 1982, Fracture analysis in northeastern Illinois and northern Indiana: University of Illinois at Urbana-Champaign, M.S. thesis, 193 p.

Friedman, S., and H.F. Weisberg, 1981, Interpreting the first eigenvalue of a correlation matrix: Educational and Psychological Measurement, v. 41, p. 11–21.

Haneberg, W.C., 2008, Using close range terrestrial digital photogrammetry for 3-D rock slope modeling and discontinuity mapping in the United States: Bulletin of Engineering Geology and Environment, p. 457–469.

Harza Engineering Company, 1986, Thorn Creek project: Thornton quarry reservoir. Geotechnical Report, Appendix B, Part 2: Chicago, Illinois, Harza Engineering Company, 43 p.

Laufeld, S., B. Sundquist, and H. Sjostrom, 1978, Megapolygonal bedrock structures in the Silurian of Gotland: Sveriges Geologiska Undersokning, Serie C, no. 759, 26 p.

Lowenstam, H.A., 1952, Some new observations on Niagaran reefs in Illinois: Transactions of the Illinois State Academy of Science, v. 45, p. 100–115. (Also Illinois State Geological Survey, Circular 183, 16 p.)

Marcotte, D., and E. Henry, 2002, Automatic joint set clustering using a mixture of bivariate normal distributions: International Journal of Rock Mechanics and Mining Sciences, v. 39, p. 323–334.

Mikulic, D.G., and J. Kluessendorf, 1999, The classic Silurian reefs of the Chicago area: 33rd Annual Meeting, North Central Section, Geological Society of America, Champaign-Urbana, Illinois, Geological Field Trip 4, April 24, 1999: Illinois State Geological Survey, Guidebook 29. 51 p.

Scheidegger, A.E., 1965, On the statistics of the orientation of bedding planes, grain axes, and similar sedimentological data: Reston, Virginia, USGS Professional Paper 525-C, p. 164–167.

Schenk, A.F. 1996. Automatic generation of DEM *in* Chapter 6, DEM extraction, editing, matching, and quality control techniques: Digital photogrammetry: An addendum to the Manual of Photogrammetry: Bethesda, Maryland, American Soci-

ety for Photogrammetry and Remote Sensing, p. 145–150.

Shuri, F.S., and S. Kelsay, 1984, Chapter 89, Rock mechanics at the Calumet Pumping Station, Chicago, Illinois: 25th Symposium on Rock Mechanics, p. 865–872.

Stohr, C., T. Kemmis, A. Stumpf, J. Thomason, and B. Curry, 2008, Stop 9: Thelen sand and gravel pits, Sedimentology of kame terrace deposits at the Thelen sand and gravel pits, northwestern Lake County, *in* Deglacial history and paleoenvironments of northeastern Illinois, 54th Midwest Friends of the Pleistocene Conference, May 16–18, 2008: Illinois State Geological Survey, Open File 2008-1, p. 164–175.

STS Consultants, Ltd., 2000, Geologic Mapping, CUP-Thornton Reservoir, Thornton, Illinois: Chicago, Illinois, U. S. Army Corps of Engineers, Chicago District, December 12, 2000, 23 p. Six appendices.

Terzaghi, R.D., 1965, Sources of error in joint surveys: Geotechnique, v. 15, p. 287–304.

Whitaker, S.T., 1988, Silurian pinnacle reef distribution in Illinois: Model for hydrocarbon exploration: Illinois State Geological Survey, Illinois Petroleum 130, 32 p.

Appendix 1: Outcrop Photogrammetry Procedures

Field Equipment

The ground control (reference points) used for georeferenced orthophotography and digitized features in three-dimensional space originates from survey data, including the measured positions of camera stations and ground control on the outcrop. These should be surveyed in absolute coordinates referenced to the current datum (the horizontal and vertical references used for conventional surveying in North America).

Surveying is accomplished using a reflectorless total station and by GNSS (Global Navigation Satellite System), commonly known as GPS (Global Positioning System) satellite surveying. Figure A1.1 shows the Leica 1200 (reflectorless) Total Station and GPS receivers and transmitters used for the surveying.

The GPS survey is the first task performed at the site in order to set ground control points for the total station. The total station is then used to survey the camera at each station where photographs are collected and to survey control points on the inaccessible outcrop for later close-range photogrammetry. When possible, the GPS survey is performed by setting up a base station at a previously surveyed location. The base station then broadcasts atmospheric and other corrections to the "rover" GPS receiver for instantaneous positioning. This permits the total station to set up and backsight on "known" ground control points so that the surveying is on ground coordinates. If the GPS base station is set up at a site without a previously surveyed point, then the surveying is more complicated.

Figure A1.1 Leica 1200 Total Station (right) and RTK GPS (center and left).

Figure A1.2 Recording a tilted image using a specially built bracket devised by Michael Dodd at the ISGS. The Nikon D80 camera is mounted on the tripod and Dodd bracket with compass and clinometer (right). The clinometer is on the left of the bracket, the compass is in the middle of the bracket, and the camera mounting plate is to the right.

Stereophotography was recorded with a Nikon D80, which has a resolution of 5.6 µm and a 28-mm f2.8 fixed-focus lens. Pixel resolution on the ground was 0.11 feet at the north flank site. The camera was mounted on the specially designed camera bracket (Figure A1.2) that has a compass, bubble level, and clinometer for setting the camera's orientation and inclination for each photograph. Some close-range photogrammetric software works best with untilted and parallel-oriented images.

Field Data Collection

Based upon previously surveyed ground control, a reflectorless total station was used to survey camera stations and reference marks on the outcrop. Ground control typically refers to points for which coordinates (i.e., position and height) are known with certainty. Reference marks on outcrops are not so well-known. A typical field deployment at another study site (Figure A1.3) shows the instruments used for outcrop photogrammetry, GPS receivers, total station, backsight prism, and camera on a tripod. At Thornton, the total station was between the camera and the outcrop at the reef apex (Figure A1.4) and offset from the camera stations at the north flank (Figure A1.5).

Spacing between camera stations is 1/7 of the distance from the wall to optimize stereoscopy. This spacing required 24 setups for the apex site with a 20-foot spacing between camera stations because the haul road is adjacent to the outcrop (Figure A1.4). A second, tilted photograph was recorded at each of the 24 stations for processing. At the north flank study site, the distance between the camera stations and the wall was 580 feet, and the spacing between the camera setups was 75 feet for the seven stations (Figure A1.5).

Camera leveling and orientation proved crucial to the collection of stereophotography for models and for subsequent interpretation. As a matter of procedure, the back (the point at which the lens meets the camera body) is the surveyed reference point.

Figure A1.3 Typical field setup with a total station and operator (left), GPS base station (middle), and RTK GPS rover (carried by operator), backsight prism (right), and camera (foreground). Photographs for stereomodels are spaced 1/7 of the distance between the outcrop and the camera station.

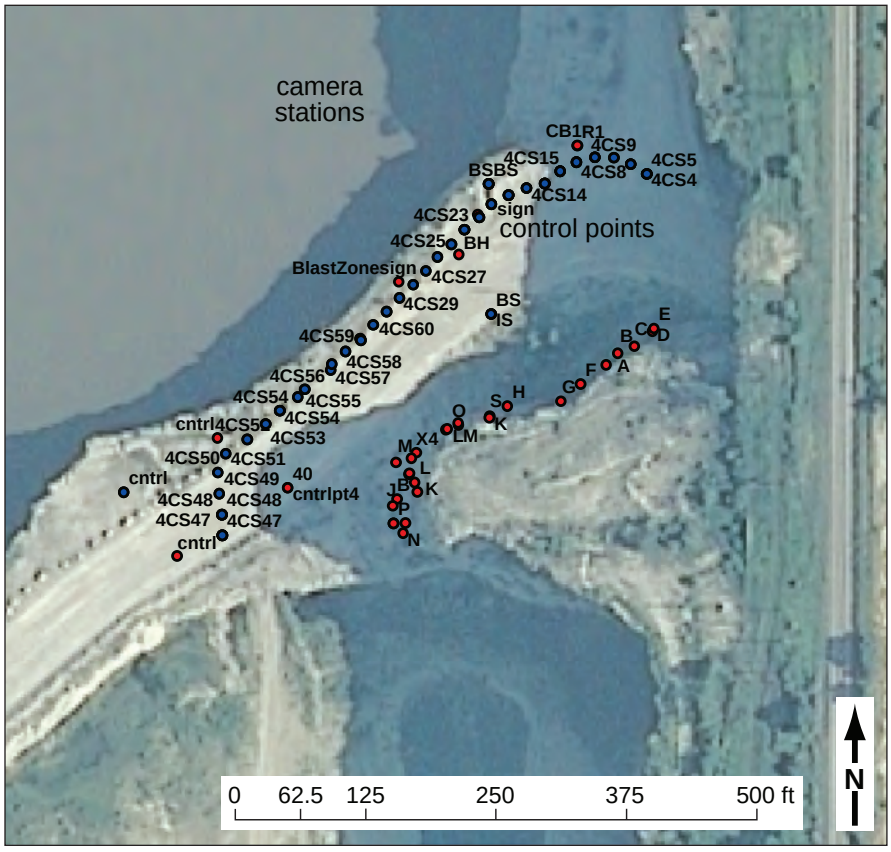

Figure A1.4 Aerial view of study site feet apex study site. The black dots are camera stations, which are closely spaced because of their proximity to the quarry wall. Reference marks are in red on the wall opposite the camera stations.

Photographic images are collected using a fixed-focus lens because of the optical characteristics needed for photogrammetric computations. The level of detail that can be observed in the photographs is a function of the camera resolution as well as the distance between the outcrop and the camera station. The distance between camera stations is dependent on access to the outcrop and mining activity.

Concurrent with or following the photography, reference points on the target outcrop or quarry wall are surveyed. This activity requires the greatest amount of field time and contributes the largest potential for error in the final stereomodels. A mosaic of the imagery is assembled in the field using Adobe Photoshop's merge feature. The merged image is opened in Adobe Illustrator, and a layer is added for marking ground control. Recognizable features on the inaccessible outcrop are identified, surveyed with the reflectorless total station, and labeled on the mosaic. A sketch and notes were made in a notebook to indicate the specific part of the feature used (e.g., tip of the upper wedge at a fracture intersection, top of cave opening, prominent bulge or pebble). This documentation proved to be the most time-consuming part of the process. The raw surveying data are reduced to position coordinates and heights in the office for use in the close-range photogrammetry software, Sirovision.

Office Procedures

If the instrument and backsight stations have not been previously surveyed, then new stations are set up, and GPS data are collected. These data are processed in one of several ways. When no base station is used, processing is done through the National Geodetic Survey's On-line Positioning User Service (OPUS), which uses multiple reference stations to calculate a position and height. Alternatively, the GPS data can be processed in Leica GeoOffice version 6 using single or multiple baselines to known reference stations.

The stereomodel is said to be georeferenced when absolute coordinates from surveyed ground control and outcrop reference marks are referenced to a

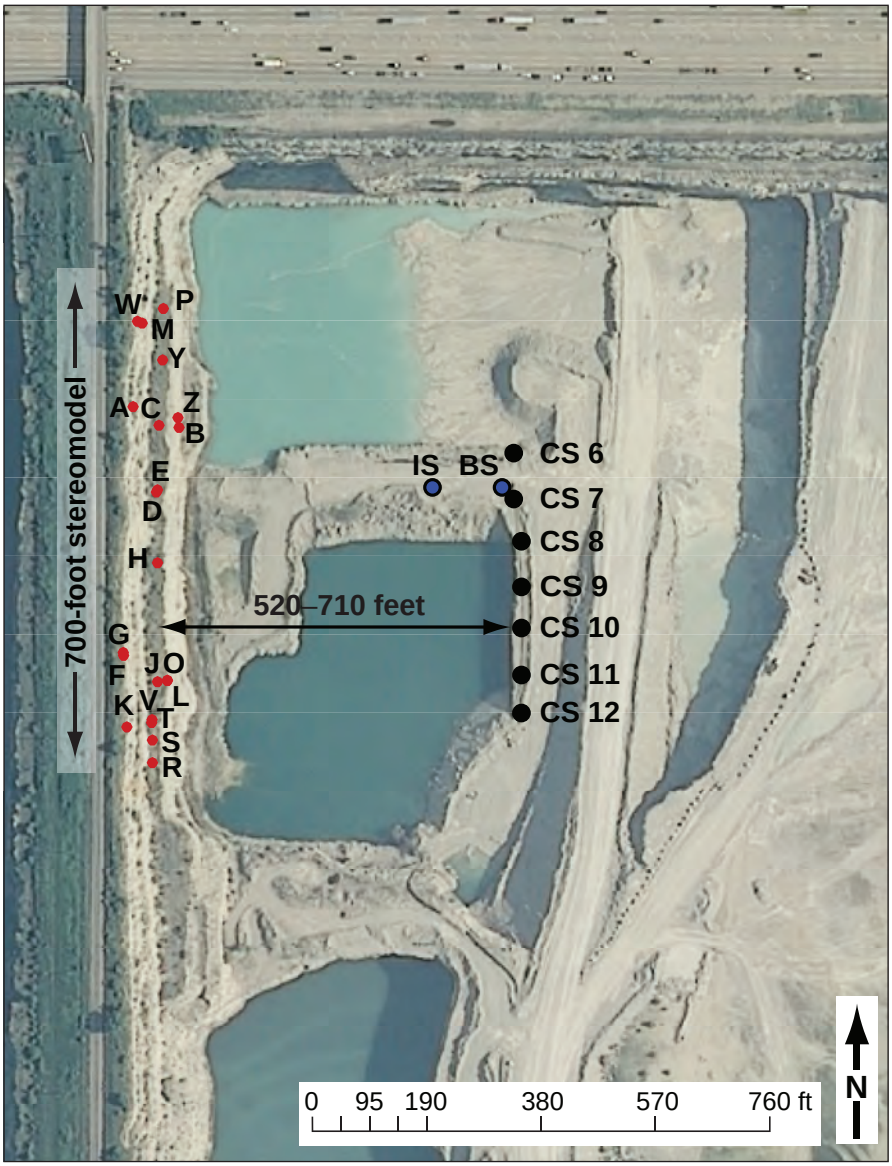

Figure A1.5 Study site north flank study site shows the 520-foot distance between the camera and the outcrop. Camera stations are numbered 6 through 12. Ground control points on the benched, vertical wall are lettered.

commonly used coordinate system such as the state plane system. Georeferencing is desirable for comparing measurements from noncontiguous outcrops.

The initial step in the photogrammetric process is to convert the digital photographs from native (or raw) image format to .tif file format using Adobe Bridge. All subsequent photogrammetric processing and delineation of features, calculation of dip and joints, and related information are obtained through Sirovision and Sirojoint software, a product of CSIRO in Australia.

The next step is to account for known characteristics of the lens and camera. The lack of calibration of the camera and lenses contributes to the error of the stereomodel and derived information. Nevertheless, use of typical focal length and camera characteristics can reduce some of the error.

A stereopair (a pair of photographs taken at adjacent stations) is selected. Figure A1.6 shows a stereopair for the three-dimensional (3-D) model of 3011-3012.

A single control point for which coordinates are known is used for georeferencing. For stereopair 3011-3012, the control point is J (red dot, Figure A1.6). Figure A1.7 shows a close-up of the control point.

Three additional points are selected to determine the relative tilt between the two images. Best results are obtained when the relative points form a triangle around the control point. Figure A1.8 shows the tilt points for 3-D model 3011-3012 as displayed by Sirovision software.

Relative orientation is used to create a stereomodel in space. The single known coordinate of the control point allows the stereomodel to be scaled and georefenced. Figure A1.9a shows an acceptable tilt output where photos are aligned in the same plane. Figure A1.9b shows poor (nonparallel) orientation of the camera in the field or a problem with the relative and absolute control points.

A rectangular portion of the image is selected for further processing (Figure A1.10) the 3-D stereomodel as a point cloud (Figure A1.11), mesh (Figure A1.12), and georeferenced, orthorectified photograph (Figure A1.13). The software works better and runs faster if the rectangle has orthogonal angles. Polygons with oblique angles do not produce good models and require a longer processing time. Common points must be fixed points (e.g., neither vegetation nor sky would be suitable).

Each pixel of the overlapping or common part of the outcrop visible in the stereopair is a different but predictable (and measurable) distance from the center of the two photographs. The difference is based on the change in distance from the outcrop to the camera. Consequently, solving the parallax equation for each common feature or pixel combination yields an exact model of the topography or DEM of the outcrop. Even subtle relief can be determined. One technique for computer-based DEM extraction for each

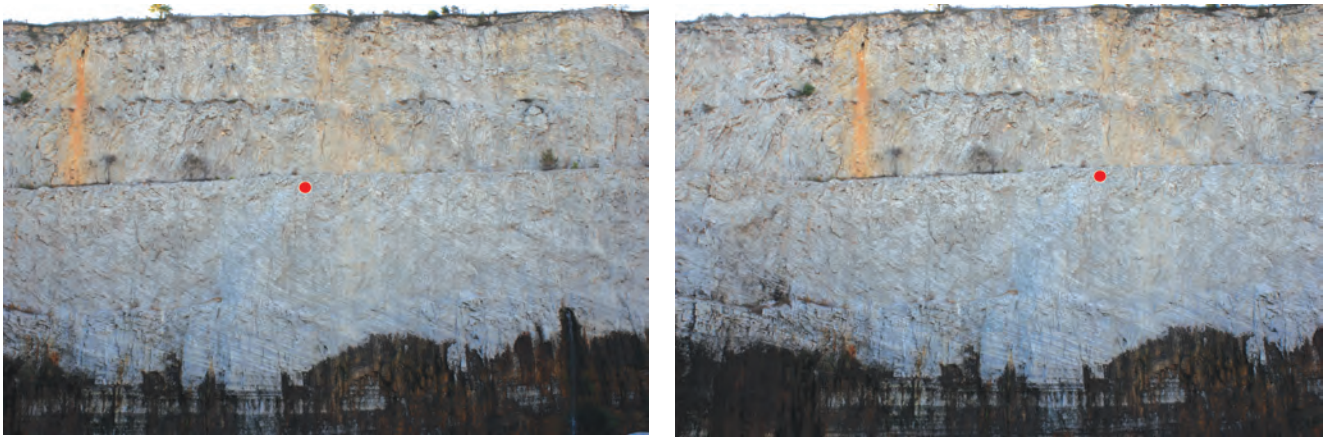

Figure A1.6 Stereopair from 3-D model 3011-3012. The image on the left was taken at camera station 12, and the image on the right was taken at camera station 11. Red dots mark the ground control point used for georeferencing and stereo-model extraction.

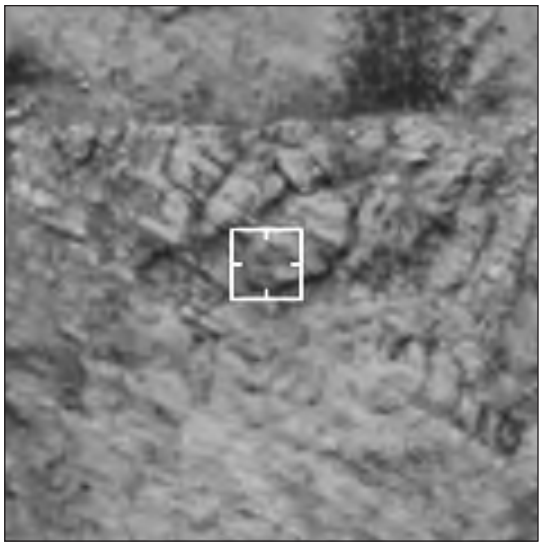

Figure A1.7 Ground control point J (within white box) for the 3-D model 3011-3012.

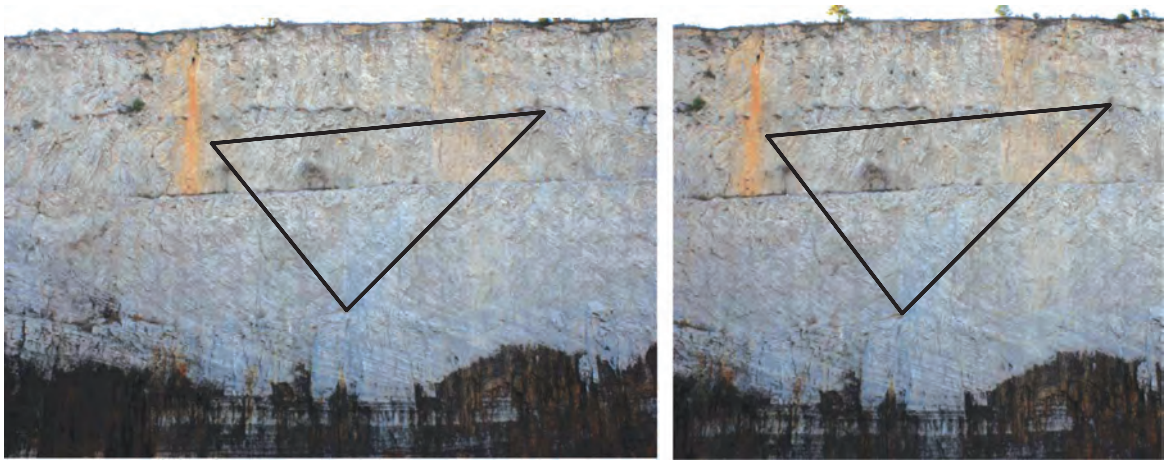

Figure A1.8 Relative tilt triangles for the 3-D model 3011-3012.

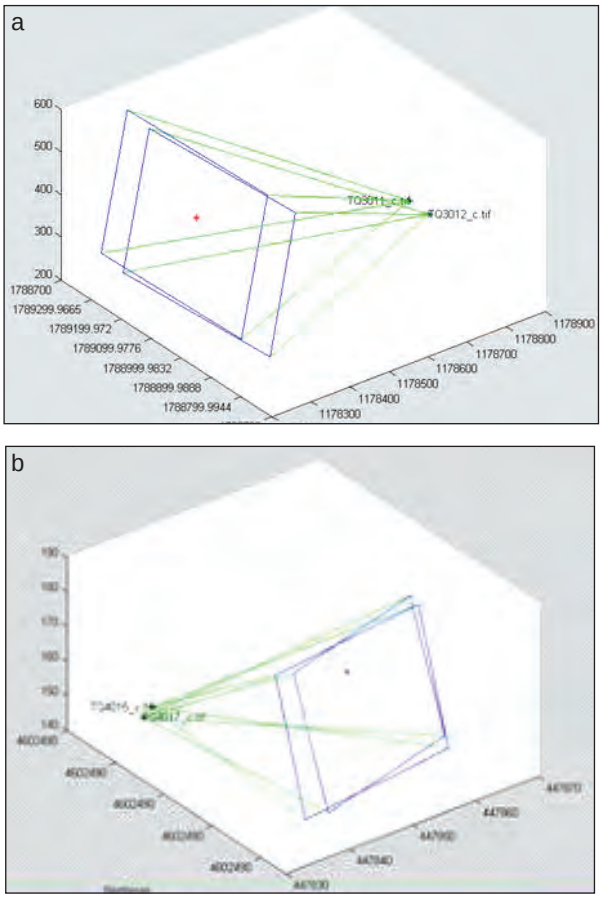

Figure A1.9 Tilt outputs from Sirovision. Image (a) is a good tilt output, and image (b), showing rectangles oblique to each other, is an undesirable tilt output.

Figure A1.10 Four points are selected on one of the stereopair photographs to delineate the 3-D model output extent.

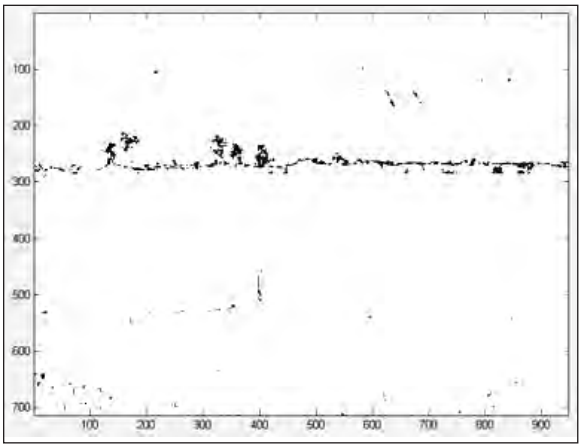

Figure A1.11 Matched and unmatched (black) pixels for the 3-D model 3011-3012. The unmatched (black) pixels in this image correspond to vegetation and the bench.

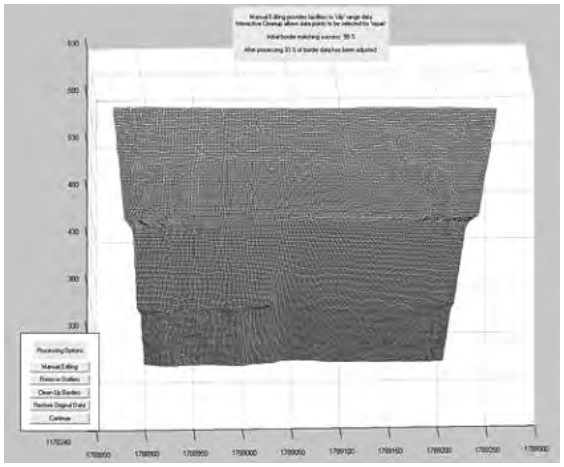

Figure A1.12 Wire mesh output for the 3-D model 3011-3012.

Figure A1.13 Final output of the 3-D model for 3011-3012.

pixel is by matching the feature edges (Schenk 1996).

The results of the pixel matching are displayed as a percentage and diagrammatically. A good matching percentage is around 98%. If the matching percentage is below 90%, the program will ask the user to rematch the data. Sirovision will rematch the images up to three times. Figure A1.11 shows the pixel matching output; positions of unmatched pixels are shown in black. Typically vegetation, ledges, and benches do not match well because of perspective and the inability of the software to resolve ambiguity of complexity of identifying moving leaves, multistory branches, etc. and parts of images that are blocked from view (Figure A1.10).

Sirovision software generates a wire mesh image that can be edited for size. Figure A1.12 shows a typical wire mesh output. Accepting the output simultaneously displays the orthophotograph draped over 3-D model and saves the model (Figure A1.13).

The individual georeferenced, orthorectified points can be exported to an ASCII file format for use in other programs, such as ArcScene. All 130,000 points or a reduced number of about 60,000 points can be exported.

Features such as lithologic contacts, facies, caves, and joints can be digitized as lines and polygons on the orthophotograph, and the x,y,z vertices can be exported to an ASCII file format using the SiroJoint program. Other information, such as the magnitude and direction of dip and the length and orientation of joints can be determined with the software, and the results can be exported to a text file.

Survey data for the camera stations, outcrop reference marks, and the digitized contacts from Sirovision points are imported to ArcMAP to be overlain on available orthophotography and digital elevation models (DEMs). The point cloud, TIN, and interpreted information from the photogrammetry-derived stereomodels are also displayed in 2.5-D in ArcScene. The display of interpreted data is the end point of the process at this time.

Appendix 2: Stereomodel 3006-3007

Appendix 2 documents the input and processing details for generating the stereomodel for the photographic stereopair 3006-3007 at the north flank of the reef at Thornton quarry (Figures A2.1 to A2.9). Joint and bedding data extracted from the stereomodel are listed in Table A2.1. Errors associated with the model are found in Table A2.2.

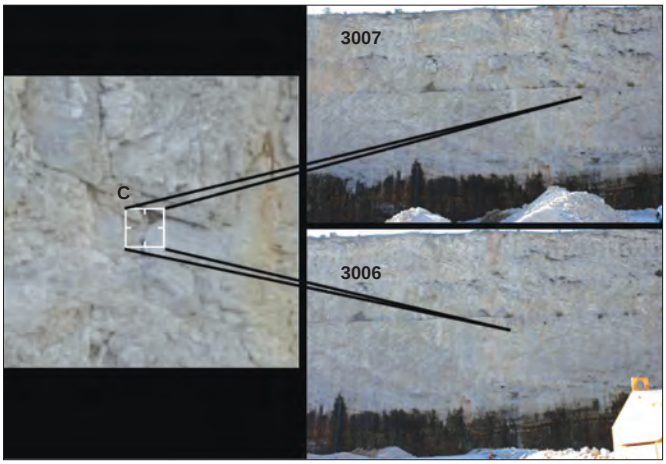

Figure A2.1 Photographic stereopair 3006-3007 showing control point C at the tip of the overhang.

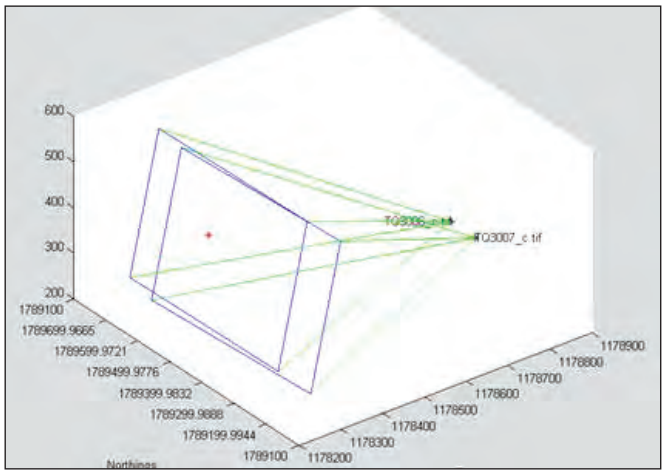

Figure A2.2 Orientation, overlap, and alignment of stereomodel 3006-3007 in relation to control point C marked by a red cross.

Figure A2.3 Area of stereomodel 3006-3007 shown in Figures A2.4, A2.5, A2.6, A2.7, and A2.9.

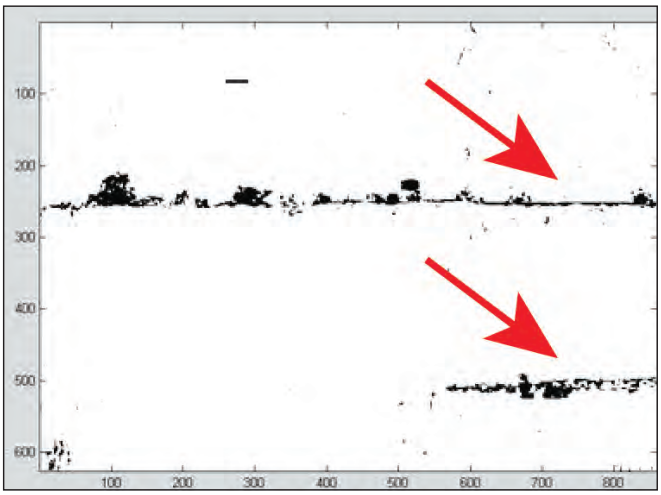

Figure A2.4 Matched (98%) and unmatched area of stereomodel 3006-3007. Most of the unmatched areas are bushes and small trees along a prominent bench above the middle of the image and a second short bench in the lower right.

Figure A2.5 Orthorectified image of 3006-3007.

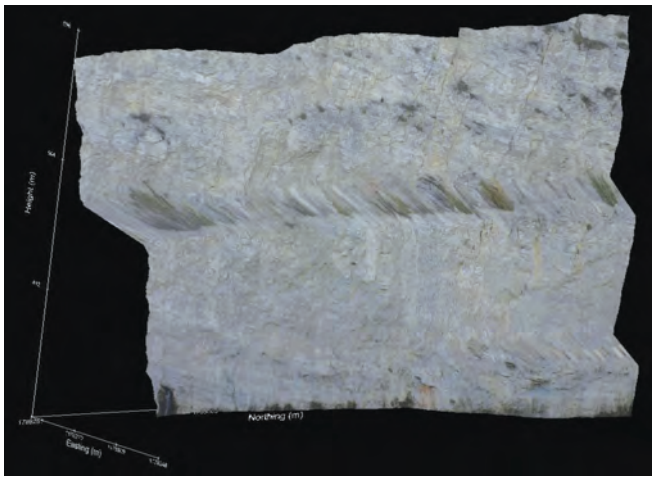

Figure A2.6 Three-dimensional stereomodel 3006-3007 with draped orthophotograph (Figure A2.5) as viewed from the lower rear showing the benches in the middle and lower right.

Table A2.1 Magnitude and direction, width, and spacing of joints as measured in model 3006-3007. Summary statistics are for joint spacing.[1]

Name	Dip	DDN	RMSE (feet)	Variance[2]	Length (feet)	Open/ closed	Joint width (feet)	Same trace on another 3-D image	Joint spacing	
									Joint	Spacing
Bedding 1	24.9	359.8	0.2	24.4	41.1	-	-	-		
Bedding 2	22	346.5	0.2	15.1	32.0	-	-	-		
Joint 1	82	81.1	0.2	31.7	23.3	closed	TCTM	Joint 5 (07-08)	1 and 3	47.3
Joint 2	72.6	139.6	0.5	15.3	22.3	closed	TCTM	-		
Joint 3	81.3	88.3	0.3	9.4	39.4	closed	0.225	Joint 6 (07-08), Joint 8 (08-09), Joint 5 (09-10)	3 and 4	68.2
Joint 4	62.3	31.4	0.7	80.1	22.1	closed	TCTM	-	4 and 12	59.6
Joint 5	57.6	88.4	0.3	8.9	14.4	closed	TCTM	-	12 and 5	66.1
Joint 6	67.1	128.7	0.5	85.5	21.2	closed	TCTM	-	6 and 2	237.3
Joint 7	83.4	230.8	0.4	89.3	17.7	closed	TCTM	-	7 and 8	16.6
Joint 8	82.1	216.9	0.6	5.4	109.0	closed	TCTM	-		
Joint 9	75.9	139.8	0.8	62.6	34.0	closed	TCTM	-	8 and 9	34.3
Joint 10	70.4	197.6	0.6	19.4	33.3	closed	TCTM	-	7 and 10	49.7
Joint 11	69.8	174.3	0.6	10.2	56.2	closed	TCTM	-	10 and 11	30.9
Joint 12	57.6	88.4	0.2	40.0	14.4	closed	TCTM	-		
									Mean	67.8
									SD	65.8
									Maximum	237.3
									Minimum	16.6
									Variance	4,329.1

[1]Abbreviations: DDN, dip direction; RMSE, root mean square error of fitted plane to a perfectly flat joint surface, i.e., a measure of roughness; 3-D, three-dimensional; TCTM, too close to measure; SD, standard deviation.
[2]Variance, the orientation of the fitted plane from a perfect surface. Larger numbers indicate a nearly straight line.

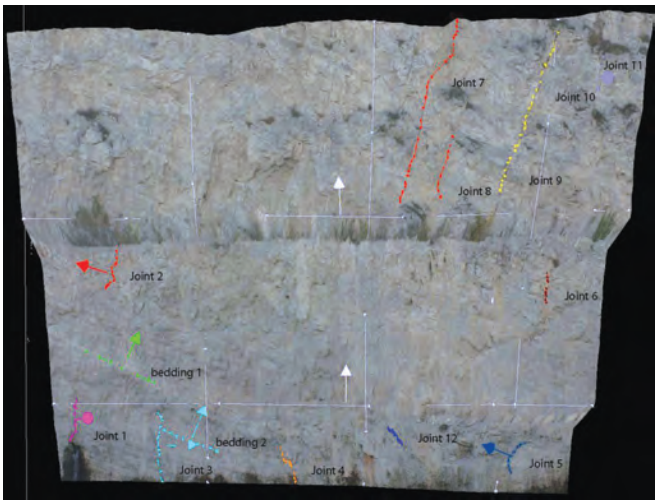

Figure A2.7 Three-dimensional image of the stereomodel and annotated orthophotograph 3006-3007 showing joint traces and bedding planes digitized in Sirovision. Most joints are nearly vertical; however, a few are curved or oriented in other directions.

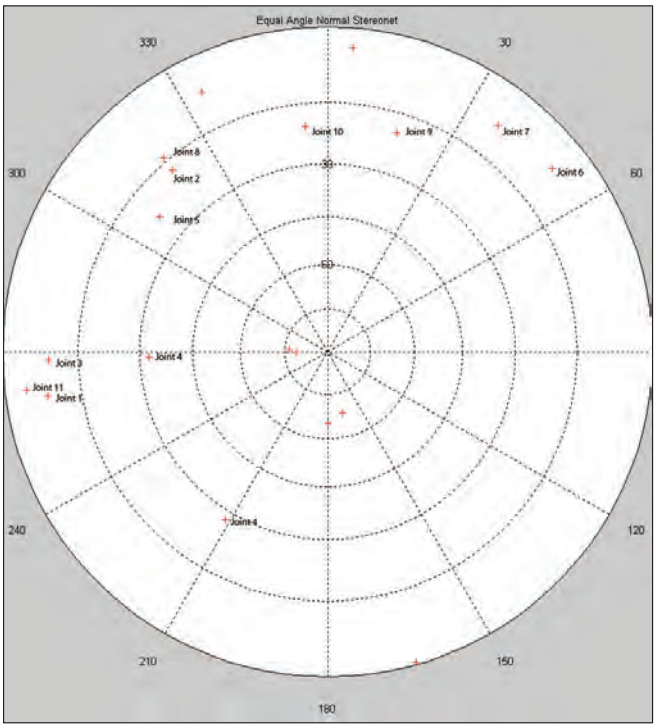

Figure A2.8 Stereonet of stereomodel 3006-3007 showing the dip magnitude and direction of joints and bedding planes listed in Table A2.1.

Table A2.2 Error (in feet) measured in model 3006-3007.

	Easting error	Northing error	Elevation error	Total error
Control point				
C	−0.8	0.1	0.3	0.8
Check point				
A	0.6	−1.3	0.5	1.6
Z	−6.4	1.0	−0.3	6.5
D	−2.0	1.8	−0.5	2.8
E	−1.6	1.6	−0.4	2.3
H	0.2	3.4	−1.1	3.6
Mean	−1.6	1.1	−0.2	2.9
Standard deviation	2.5	1.6	0.6	2.0
Maximum	0.6	3.4	0.5	6.5
Minimum	−6.4	−1.3	1.1	0.8
Variance	6.4	2.7	0.3	3.9

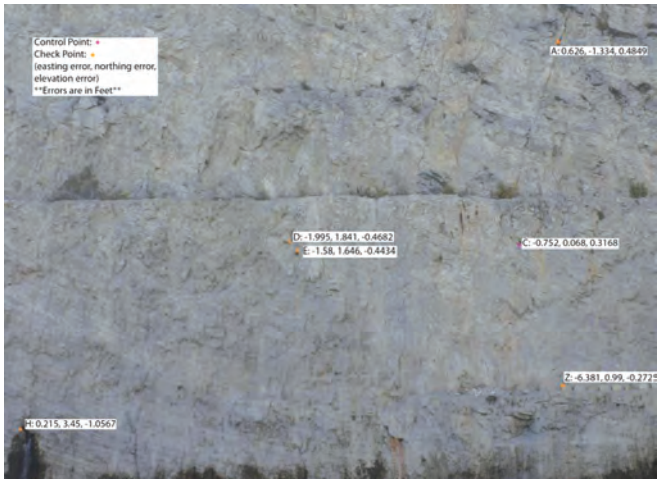

Figure A2.9 Control point C and check points for orthophotograph 3006-3007. Errors are shown in feet for easting, northing, and elevation.

Appendix 3: Stereomodel 3007-3008

Appendix 3 documents the input and processing details for generating the stereomodel for the photographic stereopair 3007-3008 at the north flank of the reef at Thornton quarry (Figures A3.1 to A3.9). Joint and bedding data extracted from the stereomodel are listed in Table A3.1. Errors associated with the model are found in Table A3.2.

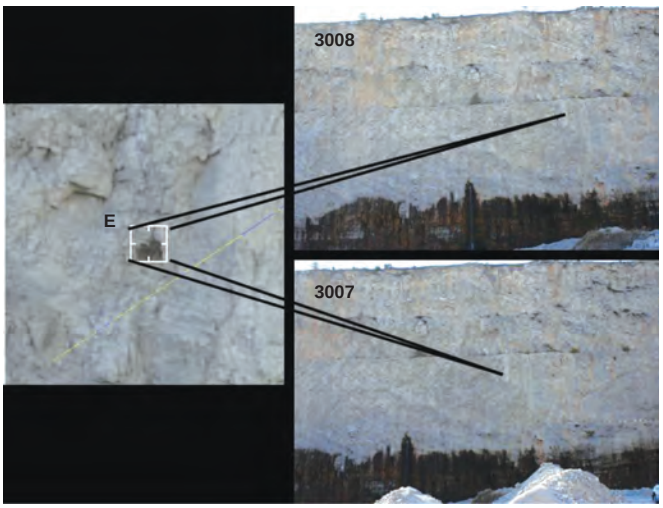

Figure A3.1 Photographic stereopair 3007-3008 showing control point E at the tip of the overhang.

Figure A3.3 Area of stereomodel 3007-3008 shown in Figures 3.4, 3.5, 3.6, 3.7, and 3.9.

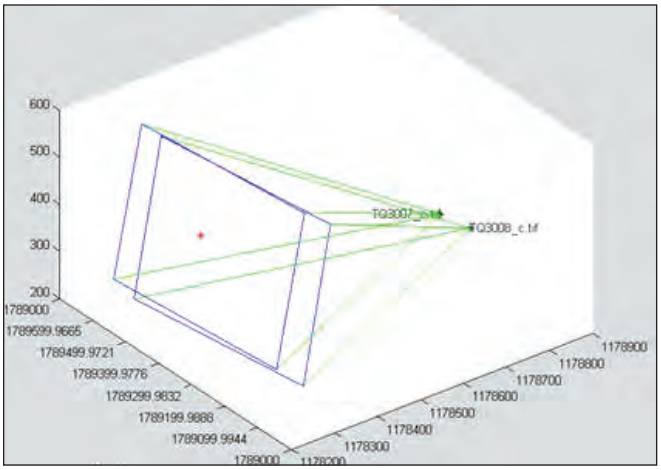

Figure A3.2 Orientation, overlap, and alignment of stereomodel 3007-3008 in relation to control point E (marked by a red cross).

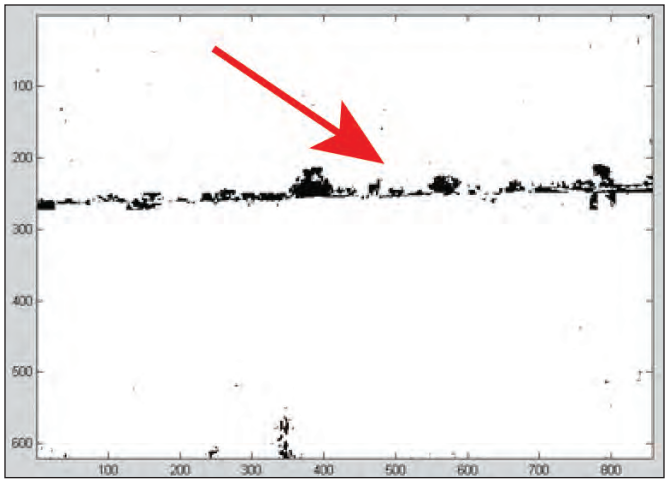

Figure A3.4 Matched (98%) and unmatched area of stereomodel 3007-3008. Most of the unmatched areas are bushes and small trees along a prominent horizontal bench across the middle of the image and a stained area with a cave issuing freely flowing water in the lower center.

Figure A3.5 Orthorectified image of 3007-3008.

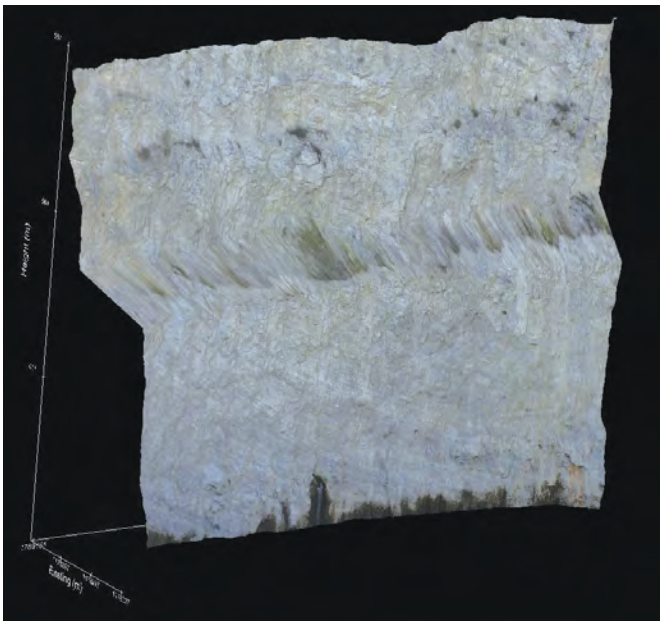

Figure A3.6 Three-dimensional stereomodel 3007-3008 with draped orthophotograph (Figure A3.5) as viewed from the lower rear showing the prominent horizontal bench in the middle.

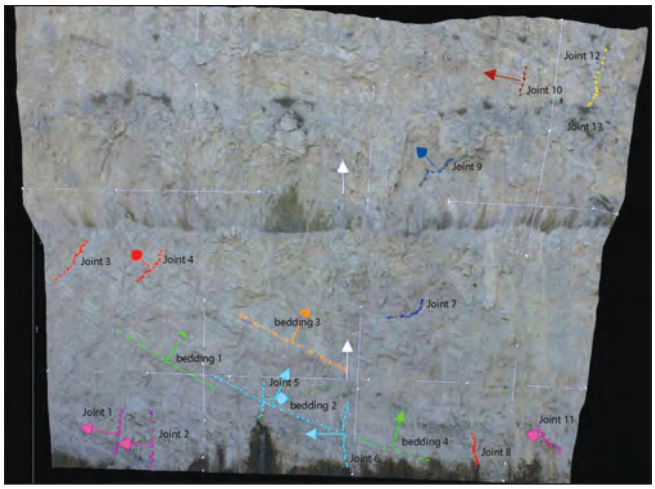

Figure A3.7 Three-dimensional image of stereomodel and annotated orthophotograph 3007-3008 showing joint traces and bedding planes digitized in Sirovision. Most joints are nearly vertical; however, a few joints are curved or oriented in other directions.

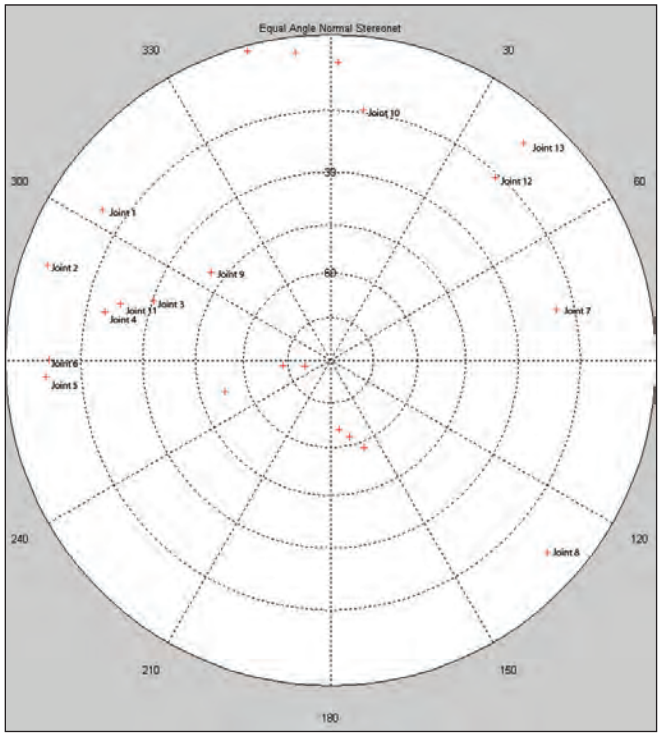

Figure A3.8 Stereonet showing dip magnitude and the direction of joints and bedding planes of stereomodel 3007-3008 in Table A3.1.

Table A3.1 Magnitude and direction, width, and spacing of joints as measured in model 3007-3008. Summary statistics are for joint spacing.[1]

Name	Dip	DDN	RMSE (feet)	Variance[2] (degrees)	Length (feet)	Open/ closed	Joint width (feet)	Same trace on another 3-D image	Joint spacing	
									Joint	Spacing
Bedding 1	32.1	339.1	0.4	62.7	62.1	-	-	-		
Bedding 2	24.3	353.2	0.7	51.2	74.7	-	-	-		
Bedding 3	27.2	346.1	0.2	8.2	65.8	-	-	-	-	-
Bedding 4	37.4	73.7	0.3	28.9	39.8	-	-	-	-	-
Joint 1	80	123.3	0.3	27.4	24.8	closed	TCTM	Joint 1 (08-09), Joint 2 (09-10)	1 and 2	18.3
Joint 2	85.1	108.5	0.2	15.1	31.4	closed	TCTM	Joint 3 (08-09), Joint 4 (09-10), Joint 4 (10-11), Joint 2 (11-12)	2 and 5	56.9
Joint 3	59.7	108.7	0.5	14.4	29.1	closed	TCTM	Joint 5 (08-09)	3 and 4	45.6
Joint 4	70.6	102	0.3	9.5	22.7	closed	TCTM	Joint 6 (08-09)	4 and 7	130.3
Joint 5	82.4	86.6	0.4	31.8	20.2	closed	TCTM	Joint 1 (06-07)	5 and 6	48.3
Joint 6	81.7	90.1	0.3	8.6	35.9	closed	0.241	Joint 3 (06-07), Joint 8 (08-09), Joint 5 (09-10)	6 and 8	73.9
Joint 7	70.7	257.4	0.6	75.3	23.8	closed	TCTM	-		
Joint 8	83.3	311.6	0.2	3.6	18.1	closed	TCTM	-	8 and 11	39.4
Joint 9	49.1	126.3	1.1	32.8	26.8	closed	TCTM	Joint 10 (09-10)	9 and 10	51.4
Joint 10	75.5	187.5	0.2	72.9	14.8	closed	TCTM	Joint 13 (08-09), Joint 11 (09-10)	10 and 12	41.1
Joint 11	67.6	104.9	0.3	19.8	23.1	open	TCTM	Joint 9 (08-09)		
Joint 12	74.1	222.1	0.5	11.8	33.9	closed	TCTM	Joint 14 (08-09)	12 and 13	12.7
Joint 13	83.5	221.7	0.5	3.2	63.1	closed	0.131	-		
									Average	51.8
									SD	32.7
									Maximum	130.3
									Minimum	12.7
									Variance	1,071.6

[1]Abbreviations: DDN, dip direction; RMSE, root mean square error of fitted plane to a perfectly flat joint surface, i.e., a measure of roughness; 3-D, three-dimensional; TCTM, too close to measure; SD, standard deviation.
[2]Variance, the orientation of the fitted plane from a perfect surface. Larger numbers indicate a nearly straight line.

Table A3.2 Error of control and check points measured in model 3007-3008.

	Easting error	Northing error	Elevation error	Total error
Control point				
E	1.7	0.1	0.0	1.7
Check point				
D	1.5	0.3	0.1	1.5
H	6.4	1.3	3.2	7.3
Mean	3.2	0.6	1.1	3.5
Standard deviation	2.8	0.7	1.8	3.3
Maximum	6.4	1.3	3.2	7.3
Minimum	1.5	0.1	0.0	1.5
Variance	7.9	0.4	3.3	11.0

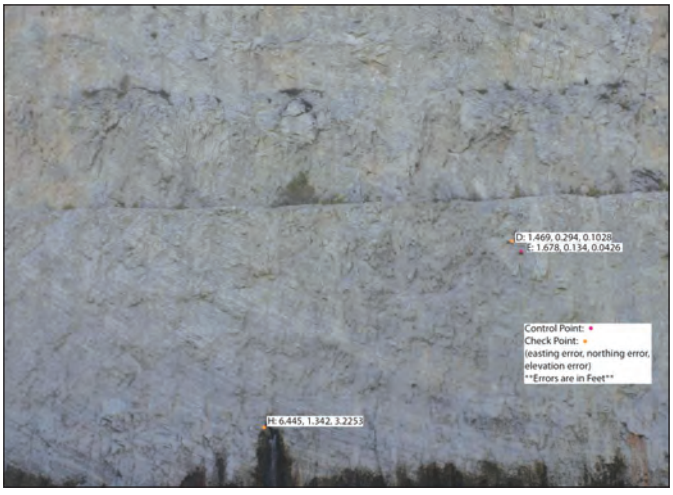

Figure A3.9 Control point E and check points for orthophotograph 3007-3008. Errors are shown in feet for easting, northing, and elevation.

Appendix 4: Stereomodel 3008-3009

Appendix 4 documents the input and processing details for generating the stereomodel for the photographic stereopair 3008-3009 at the north flank of the reef at Thornton quarry (Figures A4.1 to A4.9). Joint and bedding data extracted from the stereomodel are listed in Table A4.1. Errors associated with the model are found in Table A4.2.

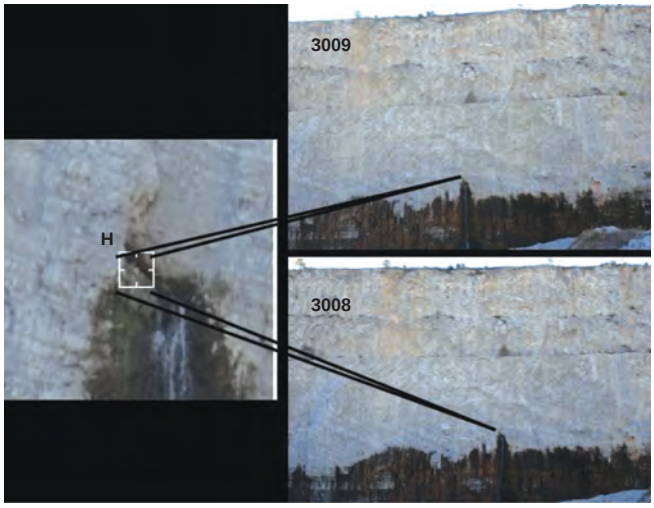

Figure A4.1 Photographic stereopair 3008-3009 showing control point H at the prominence of the underside of an open joint.

Figure A4.3 Area of stereomodel 3008-3009 shown in Figures A4.4, A4.5, A4.6, A4.7, and A4.9.

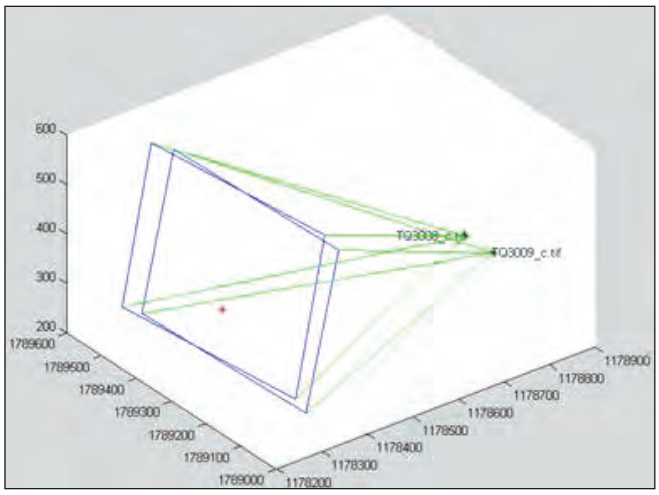

Figure A4.2 Orientation, overlap, and alignment of stereomodel 3008-3009 in relation to control point H (marked by a red cross).

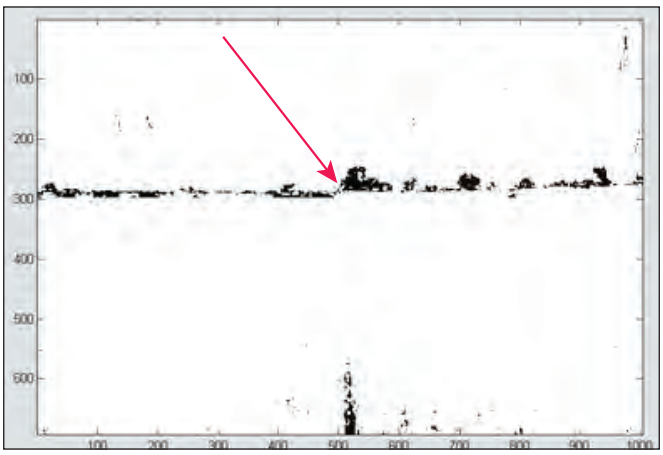

Figure A4.4 Matched (98%) and unmatched area of stereomodel 3008-3009. Most of the unmatched areas are bushes along a prominent horizontal bench at the middle of the image and a stained area in the lower middle.

Figure A4.5 Orthorectified image of 3008-3009.

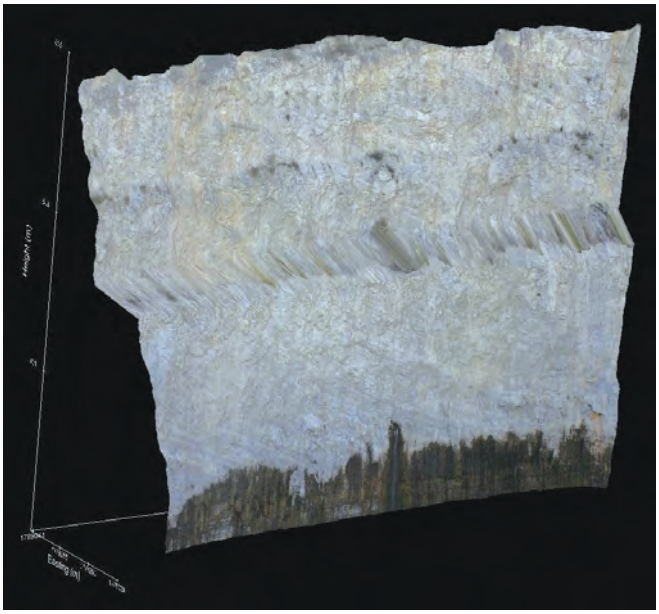

Figure A4.6 Three-dimensional stereomodel 3008-3009 with a draped orthophotograph (Figure A4.5) as viewed from the lower rear showing the prominent horizontal bench in the middle.

Figure A4.7 Three-dimensional image of stereomodel and annotated orthophotograph 3008-3009 showing joint traces and bedding planes digitized in Sirovision. Most joints are nearly vertical; however, a few joints are curved or oriented in other directions.

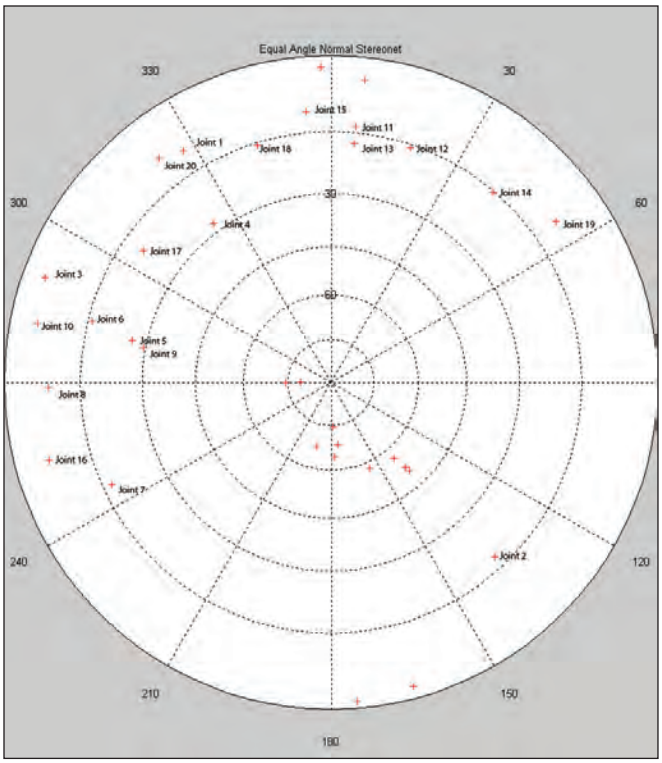

Figure A4.8 Stereonet showing dip magnitude and the direction of joints and bedding planes of stereomodel 3008-3009 in Table A4.1.

Table A4.1 Magnitude and direction, width, and spacing of joints as measured in model 3008-3009. Summary statistics are for joint spacing.[1]

Name	Dip	DDN	RMSE (feet)	Variance[2] (degrees)	Length (feet)	Open/ closed	Joint width (feet)	Same trace on another 3-D image	Joint spacing	
									Joint	Spacing
Bedding 1	25.6	356.9	0.5	9.8	48.5	-	-	-		
Bedding 2	38.2	319	0.3	93.2	41.7	-	-	-		
Bedding 3	33.7	320.5	0.3	77.9	58.2	-	-	-		
Bedding 4	39.8	318.5	0.3	88.9	62.1	-	-	-		
Bedding 5	32.1	336	0.4	95.1	59.2	-	-	-		
Bedding 6	21.7	353.8	0.3	5.7	50.8	-	-	-		
Bedding 7	22.6	12.6	0.2	9.3	55.6	-	-	-		
Bedding 8	15.5	357.4	0.4	9.7	66.7	-	-	-		
Joint 1	80.1	147.5	0.2	7.4	29.3	closed	TCTM	Joint 1 (07-08), Joint 2 (09-10)	1 and 2	11.3
Joint 2	72.4	316.8	1.5	19.3	32.6	closed	TCTM	Joint 3 (09-10), Joint 2 (07-08), Joint 4 (09-10), Joint 4 (10-11)	2 and 3	16.1
Joint 3	85.9	110.1	0.4	10.2	48.5	closed	TCTM	Joint 2 (11-12)	3 and 7	33.2
Joint 4	62.4	143.5	0.6	37.0	23.0	closed	TCTM	-	4 and 5	45.8
Joint 5	63.8	102	0.7	6.9	32.3	closed	TCTM	Joint 3 (07-08)	5 and 6	39.6
Joint 6	74.1	104.4	0.2	3.3	31.4	closed	TCTM	Joint 4 (07-08)	6 and 10	234.2
Joint 7	73	65	0.3	45.4	26.2	open	TCTM	-	7 and 8	68.3
Joint 8	81.7	89	0.3	6.1	38.4	closed	0.288	Joint 3 (06-07), Joint 6 (07-08), Joint 5 (09-10)	8 and 9	116.0
Joint 9	60.5	100.4	0.5	26.3	23.1	closed	TCTM	Joint 11 (07-08)		
Joint 10	85	101.3	0.2	20.7	28.8	closed	TCTM	-		
Joint 11	76.4	185.5	7.8	29.4	89.9	open	TCTM	-	12 and 11	18.9
Joint 12	74.4	198.7	1.2	8.4	94.0	closed	0.255	-	14 and 12	11.8
Joint 13	72.5	185.5	0.6	61.4	20.1	closed	TCTM	Joint 10 (07-08), Joint 11 (09-10)	15 and 13	154.0
Joint 14	74.8	220.5	0.6	70.3	36.0	closed	TCTM	Joint 12 (07-08)	13 and 14	42.5
Joint 15	79.5	174.7	0.6	6.1	68.3	closed	TCTM	Joint 9 (09-10), Joint 9 (10-11)	16 and 15	14.7
Joint 16	83.7	74.6	0.4	76.7	25.8	closed	TCTM	-	18 and 16	121.5
Joint 17	70	125.1	0.9	4.7	36.0	closed	TCTM	-	20 and 17	71.1
Joint 18	74.5	162.7	0.4	11.7	42.9	closed	TCTM	Joint 8 (09-10), Joint 8 (10-11), Joint 8 (11-12)	19 and 18	5.8
Joint 19	80.5	234.4	0.3	92.6	38.7	closed	TCTM	Joint 12 (09-10), Joint 7 (10-11), Joint 7 (11-12)		
Joint 20	81.7	142.5	1.2	14.2	60.5	closed	TCTM	Joint 7 (09-10), Joint 6 (10-11), Joint 9 (11-12		
									Average	62.8
									SD	63.8
									Maximum	234.2
									Minimum	5.8
									Variance	4,074.4

[1]Abbreviations: DDN, dip direction; RMSE, root mean square error of fitted plane to a perfectly flat joint surface, i.e., a measure of roughness; TCTM, too close to measure; SD, standard deviation.
[2]Variance, the orientation of the fitted plane from a perfect surface. Larger numbers indicate a nearly straight line.

Table A4.2 Error of control and check points measured in model 3008-3009; measurements in feet.

	Easting error	Northing error	Elevation error	Total error
Control point				
H	−0.5	−1.2	1.6	2.1
Check point				
D	−4.5	−2.4	1.8	5.4
E	−3.9	−2.0	1.9	4.8
F	−3.0	−0.1	0.9	3.1
G	−3.1	1.6	−0.3	3.5
Mean	−3.0	−0.8	1.2	3.8
Standard deviation	1.5	1.6	0.9	1.3
Maximum	−0.5	1.6	1.9	5.4
Minimum	−4.5	−2.4	−0.3	2.1
Variance	2.3	2.7	0.8	1.8

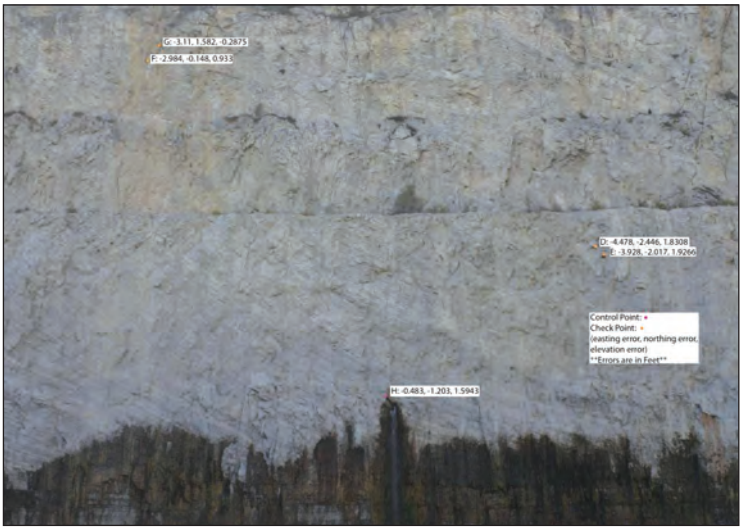

Figure A4.9 Control point H immediately above a small cave issuing water and check points for orthophotograph 3008-3009. Errors are shown in feet for easting, northing, and elevation.

Appendix 5: Stereomodel 3009-3010

Appendix 5 documents the input and processing details for generating the stereomodel for the photographic stereopair 3009-3010 at the north flank of the reef at Thornton quarry (Figure A5.1 to A5.8).

Joint and bedding data extracted from the stereomodel are listed in Table A5.1. Errors associated with the model are found in Table A5.2.

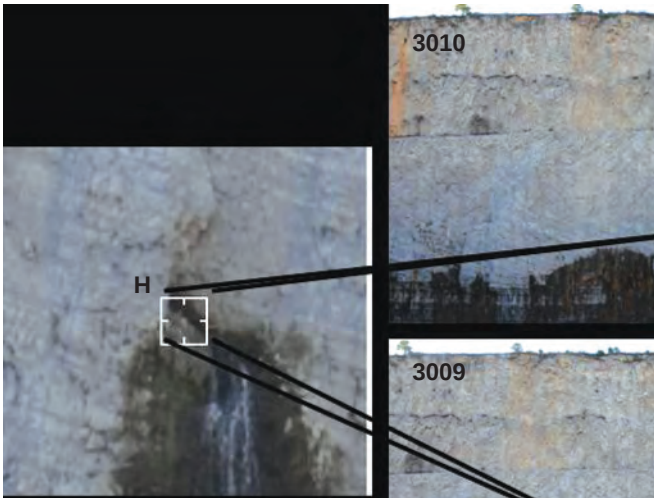

Figure A5.1 Photographic stereopair 3009-3010 showing control point H at a prominence of the underside of an open joint.

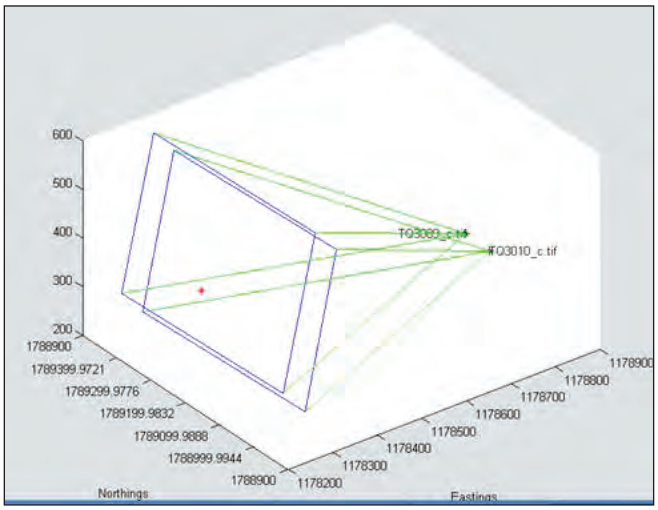

Figure A5.2 Orientation, overlap, and alignment of stereomodel 3009-3010 in relation to control point H (marked by a red cross).

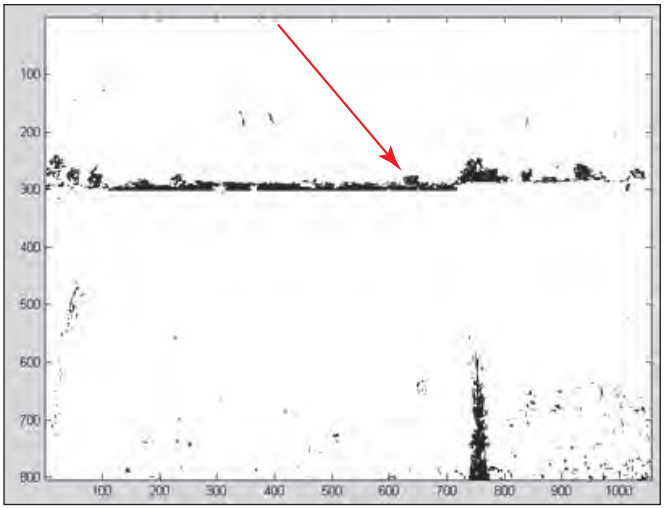

Figure A5.3 Matched (98%) and unmatched area of stereomodel 3009-3010. Most of the unmatched areas are small trees and bushes on a prominent horizontal bench above the middle of the image and a stained area in lower right.

Figure A5.4 Orthorectified image of 3009-3010.

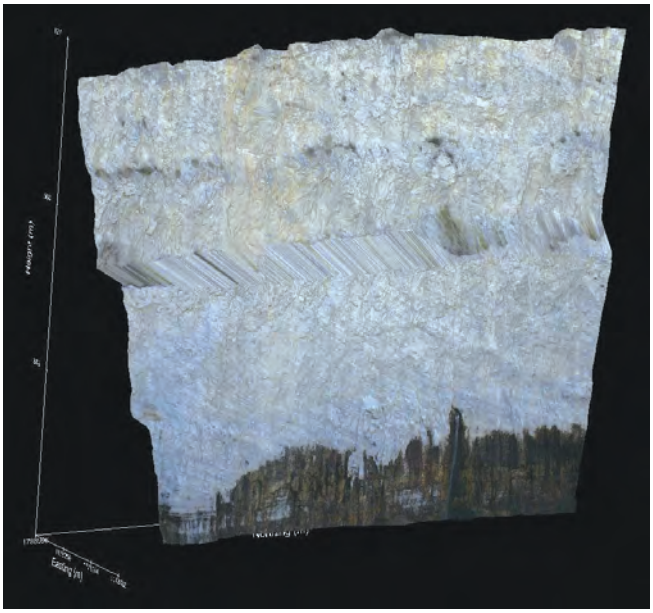

Figure A5.5 Three-dimensional stereomodel 3009-3010 with a draped orthophotograph (Figure A5.4) as viewed from the lower rear showing the prominent horizontal bench in the middle and a smaller, less prominent bench in the lower left.

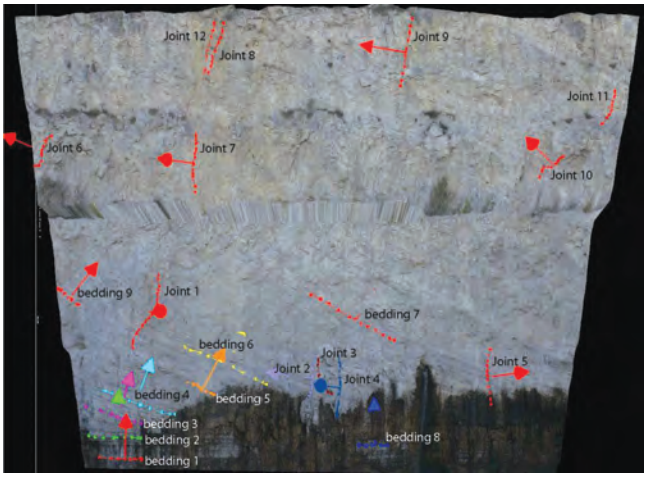

Figure A5.6 Three-dimensional image of steromodel and annotated orthophotograph 3009-3010 showing joint traces and bedding planes digitized in Sirovision. Most joints are near vertical, however, a few joints are curved or oriented in other directions.

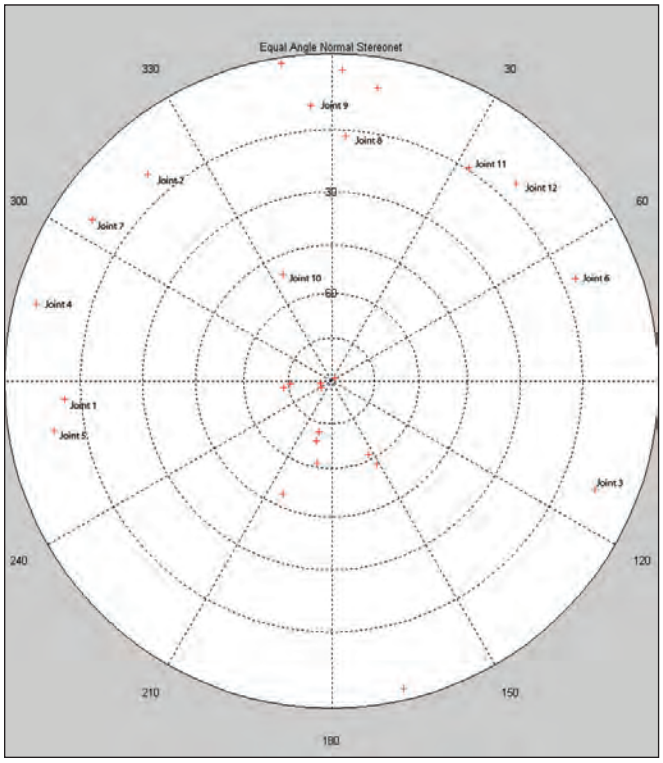

Figure 5.7 Stereonet showing dip magnitude and direction of joints and bedding planes of stereomodel 3009-3010 listed in Table A5.1.

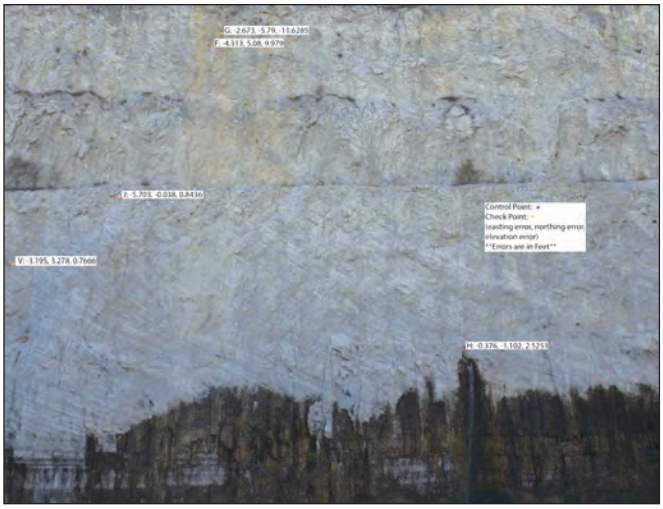

Figure 5.8 Control point H and check points for orthophotograph 3009-3010. Errors shown in feet for easting, northing, and elevation.

Table A5.1 Magnitude and direction, width, and spacing of joints as measured in model 3009-3010. Summary statistics are for joint spacing.[1]

Name	Dip	DDN	RMSE (feet)	Variance[2] (degrees)	Length (feet)	Open/ closed	Joint width (feet)	Same trace on another 3-D image	Joint spacing	
									Joint	Spacing
Bedding 1	16.7	81.7	0.1	8.0	30.8	-	-	-		
Bedding 2	4.2	56.5	0.4	14.4	38.0	-	-	-		
Bedding 3	18.2	13.7	2.4	6.1	43.5	-	-	-		
Bedding 4	21.3	13.8	0.7	6.2	62.5	-	-	-		
Bedding 5	28.4	10	0.3	80.5	22.0	-	-	-		
Bedding 6	28.2	333.3	0.5	92.0	66.0	-	-	-		
Bedding 7	32.3	331.3	0.1	5.0	69.2	-	-	-		
Bedding 8	1.6	231.9	0.1	5.0	69.2	-	-	-		
Bedding 9	41.2	23	0.2	28.0	20.1	-	-	-		
Joint 1	78.5	86	0.8	12.0	59.3	closed	TCTM	-	1 and 2	120.9
Joint 2	80.3	138.3	0.4	18.0	29.3	closed	TCTM	Joint 1 (08-09), Joint 1 (07-08)	2 and 3	104.6
Joint 3	82.1	292.4	0.4	14.0	28.3	closed	TCTM	Joint 2 (08-09)	3 and 4	6.1
Joint 4	86	104.6	0.2	11.0	45.2	closed	TCTM	Joint 3 (08-09), Joint 2 (07-08), Joint 4 (10-11), Joint 2 (11-12)	4 and 5	15.9
Joint 5	81.4	79.8	0.4	22.5	40.4	closed	0.114	Joint 8 (08-09), Joint 6 (07-08)		
Joint 6	77.8	247.3	0.8	77.4	26.7	closed	0.138	-	6 and 7	110.2
Joint 7	82.7	124	0.4	14.7	42.8	closed	TCTM	Joint 20 (08-09), Joint 6 (10-11), Joint 9 (11-12)	7 and 10	249.3
Joint 8	73.7	183.4	0.7	34.9	36.6	closed	TCTM	Joint 18 (08-09), Joint 8 (10-11), Joint 8 (11-12)	8 and 9	136.6
Joint 9	80.2	175.7	0.3	9.7	48.9	closed	TCTM	Joint 15 (08-09), Joint 9 (10-11)	9 and 11	153.3
Joint 10	39.3	155.5	1.0	49.0	27.4	closed	TCTM	Joint 9 (07-08)		
Joint 11	75.5	212.9	0.3	7.7	27.5	open	TCTM	Joint 10 (07-08)		
Joint 12	79.1	223.1	0.3	56.3	37.3	closed	TCTM	Joint 19 (08-09), Joint 7 (10-11), Joint 7 (11-12)	12 and 8	5.7
									Mean	100.3
									SD	80.5
									Maximum	249.3
									Minimum	5.7
									Variance	6,476.6

[1]Abbreviations: DDN, dip direction; RMSE, root mean square error of fitted plane to a perfectly flat joint surface, i.e., a measure of roughness; TCTM, too close to measure; SD, standard deviation.
[2]Variance, the orientation of the fitted plane from a perfect surface. Larger numbers indicate a nearly straight line.

Table A5.2 Error of control and check points measured in model 3009-3010; measurements in feet.

	Easting error	Northing error	Elevation error	Total error
Control point				
H	−0.4	−1.1	2.5	2.8
Check point				
F	−4.3	5.1	10.0	12.0
G	−2.7	−5.8	−11.6	13.3
J	−5.7	0.0	0.8	5.8
V	−3.2	3.3	0.8	4.6
Mean	−3.3	0.3	0.5	7.7
Standard deviation	2.0	4.2	7.8	4.7
Maximum	−0.4	5.1	10.0	13.3
Minimum	−5.7	−5.8	−11.6	2.8

Appendix 6: Stereomodel 3010-3011

Appendix 6 documents the input and processing details for generating the stereomodel for the photographic stereopair 3010-3011 at the north flank of the reef at Thornton quarry (Figure A6.1 to A6.7. Joint and bedding data extracted from the stereomodel are listed in Table A6.1. Errors associated with the model are found in Table A6.2.

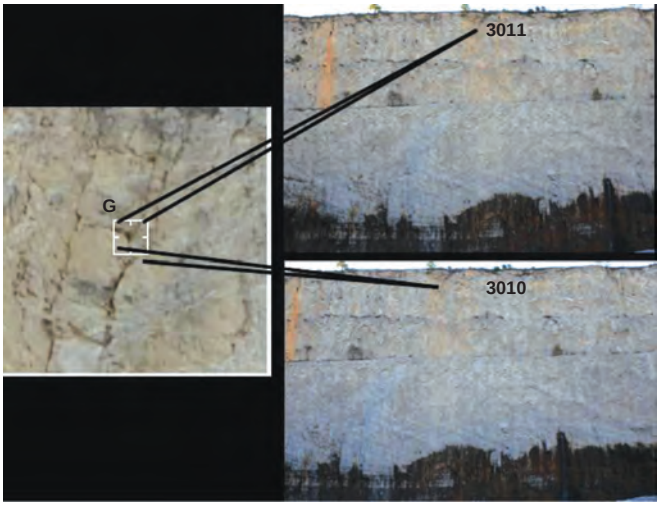

Figure A6.1 Photographic stereopair 3010-3011 showing control point G at the enlarged terminus of joint.

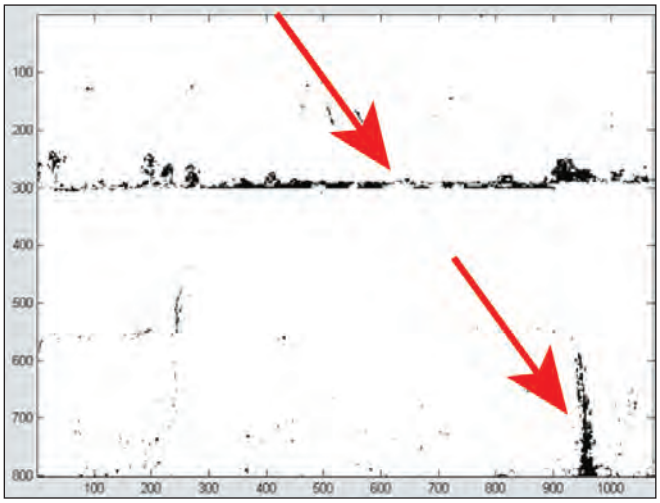

Figure A6.2 The matched (98%) and unmatched area of stereomodel 3010-3011. Most of the unmatched areas are a prominent bench with small trees and bushes above the middle of the image and a stained area in the lower right.

Figure A6.3 Orthorectified image of 3010-3011.

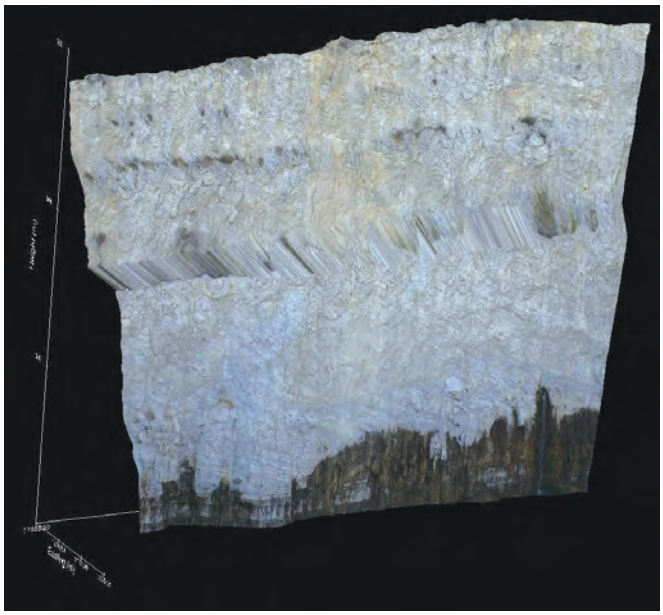

Figure A6.4 Three-dimensional stereomodel 3010-3011 with a draped orthophotograph (Figure A6.3) as viewed from the lower rear showing the prominent horizontal bench in the middle.

Table A6.1 Magnitude and direction, width, and spacing of joints as measured in model 3010-3011. Summary statistics are for joint spacing.[1]

Name	Dip	DDN	RMSE (feet)	Variance[2] (degrees)	Length (feet)	Open/ closed	Joint width (feet)	Same trace on another 3-D image	Joint spacing	
									Joint	Spacing
Bedding 1	6.2	319.7	0.4	2.3	114.7	-	-	-		
Bedding 2	17.7	33.4	0.2	2.9	52.0	-	-	-		
Bedding 3	23.9	23.7	0.3	4.0	58.6	-	-	-		
Bedding 4	28.1	236.0	1.5	16.5	95.6	-	-	-		
Bedding 5	3.0	277.0	0.4	10.2	69.2	-	-	-		
Bedding 6	25.6	353.7	0.4	7.4	54.7	-	-	-		
Joint 1	84.0	60.6	0.2	10.7	30.7	closed	TCTM	Joint 4 (11-12)	1 and 2	115.4
Joint 2	80.4	142.3	0.4	31.2	24.7	closed	TCTM	-		
Joint 3	78.3	38.8	0.8	70.4	26.0	closed	TCTM	-	3 and 4	32.7
Joint 4	86.5	94.7	0.2	7.4	37.5	closed	TCTM	Joint 2 (07-08), Joint 3 (08-09), Joint 4 (09-10), Joint 2 (11-12),		
Joint 5	80.7	114.8	0.2	62.6	25.5	closed	0.1	Joint 6 (11-12)	5 and 6	105.0
Joint 6	79.9	146.4	3.0	7.4	55.4	closed	TCTM	Joint 20 (08-09), Joint 7 (09-10), Joint 9 (11-12)		
Joint 7	81.6	239.9	0.5	81.1	37.1	closed	TCTM	Joint 19 (08-09), Joint 12 (09-10), Joint 7 (11-12)	7 and 8	5.7
Joint 8	73.2	174.4	0.3	12.8	37.2	closed	TCTM	Joint 18 (08-09), Joint8 (09-10), Joint 8 (11-12)	8 and 9	133.2
Joint 9	79.6	178.0	0.5	4.9	63.5	closed	TCTM	Joint 15 (08-09), Joint 9 (09-10)		
									Mean	78.4
									SD	55.8
									Maximum	133.2
									Minimum	5.7
									Variance	3,114.1

[1]Abbreviations: DDN, dip direction; RMSE, root mean square error of fitted plane to a perfectly flat joint surface, i.e., a measure of roughness; TCTM, too close to measure; SD, standard deviation.
[2]Variance, the orientation of the fitted plane from a perfect surface. Larger numbers indicate a nearly straight line.

Table A6.2 Error of control and check points measured in model 3010-3011; measurements in feet.

Control point	Easting error	Northing error	Elevation error	Total error
G	1.1	−0.1	−0.3	1.2
Check point				
F	0.8	−2.3	0.8	2.6
H	2.8	−3.1	3.3	5.3
J	−1.2	−0.5	2.1	2.5
K	1.8	2.5	−1.2	3.3
S	−0.3	1.9	2.4	3.1
T	−0.7	1.4	2.9	3.3
V	−0.8	2.8	3.0	4.2
Mean0.4	0.3	1.6	3.2	
Standard deviation	1.4	2.2	1.7	1.2
Maximum	2.8	2.8	3.3	5.3
Minimum	−1.2	−3.1	−1.2	1.2
Variance	2.0	4.9	2.8	1.5

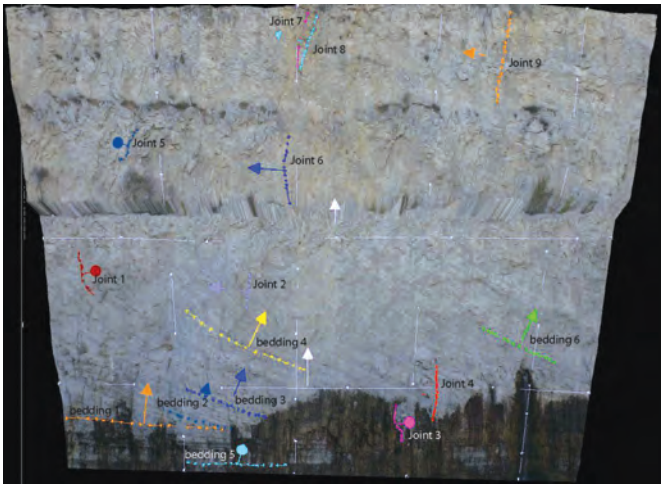

Figure A6.5 Three-dimensional image of a stereomodel and an annotated orthophotograph 3010-3011 showing joint traces and bedding planes digitized in Sirovision. Most joints are nearly vertical.

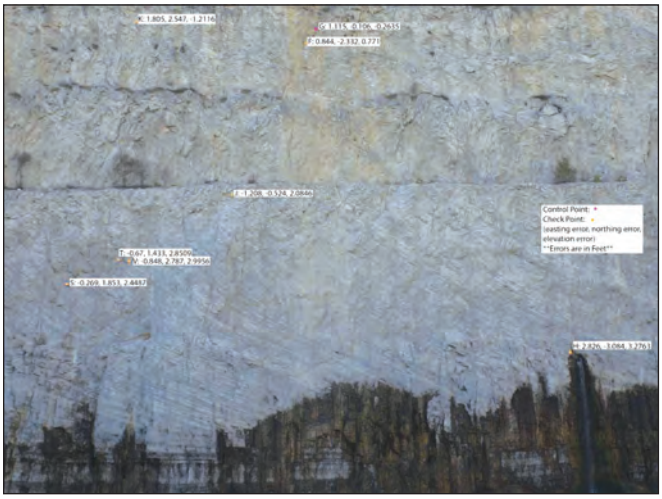

Figure A6.7 Control point G and check points for orthophotograph 3010-3011. Check point H is at a cave issuing flowing water in lower right. Errors are shown in feet for easting, northing, and elevation.

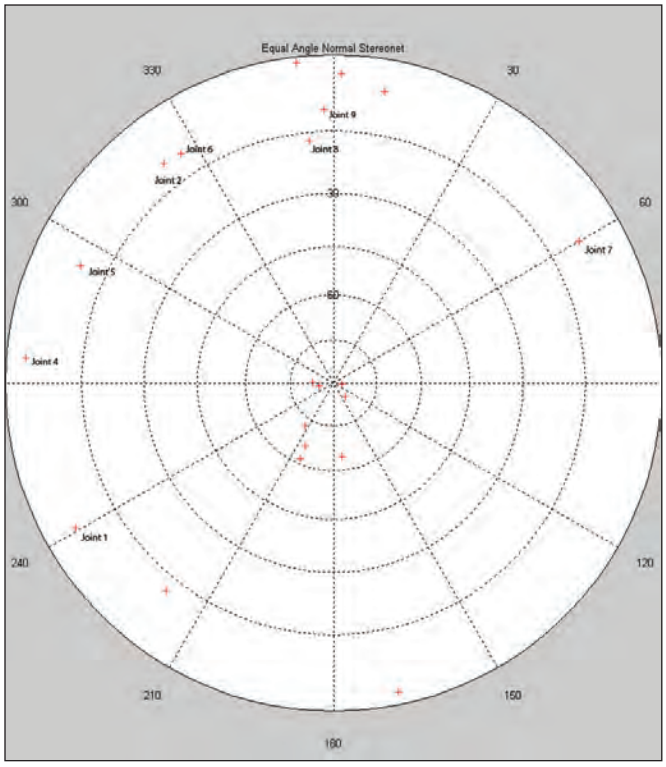

Figure A6.6 Stereonet showing dip magnitude and the direction of the joints and bedding planes of stereomodel 3010-3011 listed in Table A6.1.

Appendix 7: Stereomodel 3011-3012

Appendix 7 documents the input and processing details for generating the stereomodel for the photographic stereopair 3011-3012 at the north flank of the reef at Thornton quarry (Figures A7.1 to A7.9). Joint and bedding data extracted from the stereomodel are listed in Table A7.1. Errors associated with the model are found in Table A7.2.

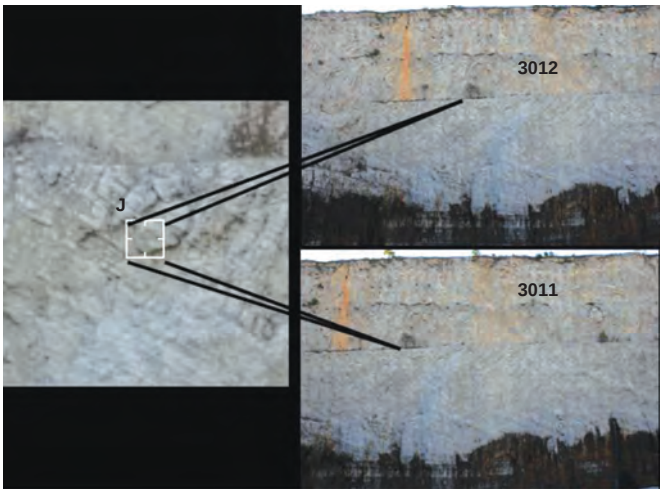

Figure 7A.1 Photographic stereopair 3011-3012 showing control point J at the top of the overhang.

Figure A7.3 Area of stereomodel 3011-3012 shown in Figures A7.4, A7.5, A7.6, A7.7, and A7.9.

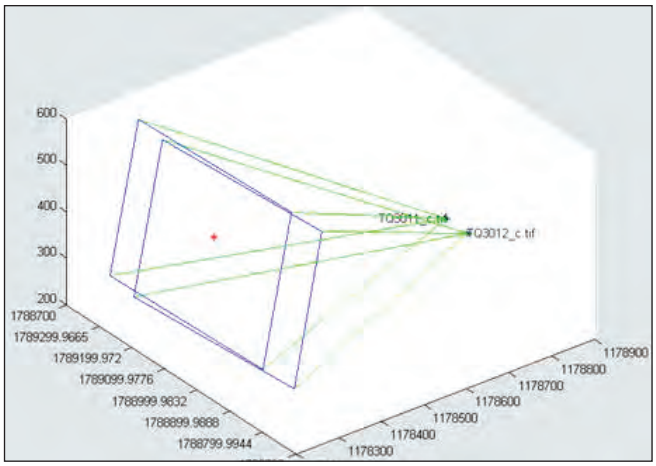

Figure A7.2 Orientation, overlap, and alignment of stereomodel 3011-3012 in relation to control point J (marked by a red cross).

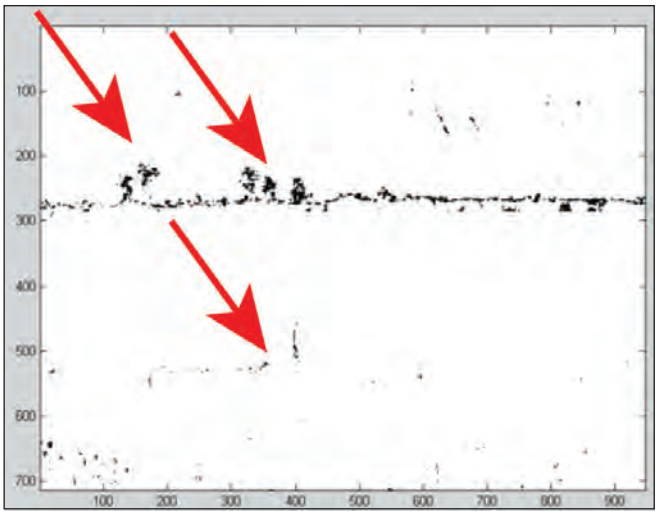

Figure A7.4 Matched (98%) and unmatched area of stereomodel 3011-3012. Most of the unmatched areas are a prominent horizontal bench with small trees at the middle of the image and a stained area with an indistinct bench in the lower middle.

Table 7.1 Magnitude and direction, width, and spacing of joints as measured in model 3011-3012. Summary statistics are for joint spacing.[1]

Name	Dip	DDN	RMSE (feet)	Variance[2] (degrees)	Length (feet)	Open/ closed	Joint width (feet)	Same trace on another 3-D image	Joint spacing	
									Joint	Spacing
Bedding 1	22.3	29.3	0.9	14.6	89.4	-	-	-		
Bedding 2	40.2	308.6	1.2	89.0	85.5	-	-	-		
Bedding 3	20.6	3	0.2	4.3	45.6	-	-	-	-	-
Bedding 4	33.2	335.8	0.2	92.2	47.1	-	-	-	-	-
Joint 1	83.4	133.7	0.3	12.7	41.9	closed	TCTM	-	1 and 2	205.2
Joint 2	85.4	99.4	0.2	7.7	38.5	closed	TCTM	Joint 2 (07-08), Joint 3 (08-09), Joint 2 (09-10), Joint 4 (10-11)		
Joint 3	80.1	51.3	0.7	63.9	23.8	closed	TCTM	-	3 and 4	69.4
Joint 4	81.8	61.8	0.4	8.8	32.4	closed	TCTM	Joint 1 (10-11)		
Joint 5	56.4	143.6	1.3	43.8	38.3	closed	TCTM	-	5 and 6	43.9
Joint 6	67.5	152.3	0.8	40.3	27.3	closed	0.253	Joint 5 (10-11)	6 and 9	105.4
Joint 7	81.3	196.8	0.2	17.1	20.9	closed	TCTM	Joint 19 (08-08), Joint 12 (09-10), Joint 7 (10-11)	7 and 8	5.6
Joint 8	74.8	165.1	0.6	10.1	25.4	closed	TCTM	Joint 18 (08-09), Joint 8 (09-10), Joint 8 (10-11)		
Joint 9	82	126.3	0.3	11.9	34.4	closed	TCTM	Joint 20 (08-09), Joint 7 (09-10), Joint 6 (10-11)		
									Mean	85.9
									SD	76.0
									Maximum	205.2
									Minimum	5.6

[1]Abbreviations: DDN, dip direction; RMSE, root mean square error of fitted plane to a perfectly flat joint surface, i.e., a measure of roughness; TCTM, too close to measure; SD, standard deviation.
[2]Variance, the orientation of the fitted plane from a perfect surface. Larger numbers indicate a nearly straight line.

Figure A7.5 Orthorectified image of 3011-3012.

Table 7.2 Error of control and check points measured in model 3011-3012; measurements in feet.

	Easting error	Northing error	Elevation error	Total error
Control point				
J	−1.5	0.0	−0.1	1.5
Check point				
R	−0.1	8.0	−0.8	8.1
F	1.6	−2.1	−2.4	5.3
G	2.2	0.2	−3.6	4.2
K	2.3	3.2	−4.5	6.0
S	−1.6	2.3	0.1	2.8
T	−1.1	1.9	0.6	2.3
V	−1.6	4.1	0.5	4.4
Mean0.0	2.2	−1.3	4.1	
Standard deviation	1.7	3.1	2.0	2.1
Maximum	2.3	8.0	0.6	8.1
Minimum	−1.6	−2.1	−4.5	1.5

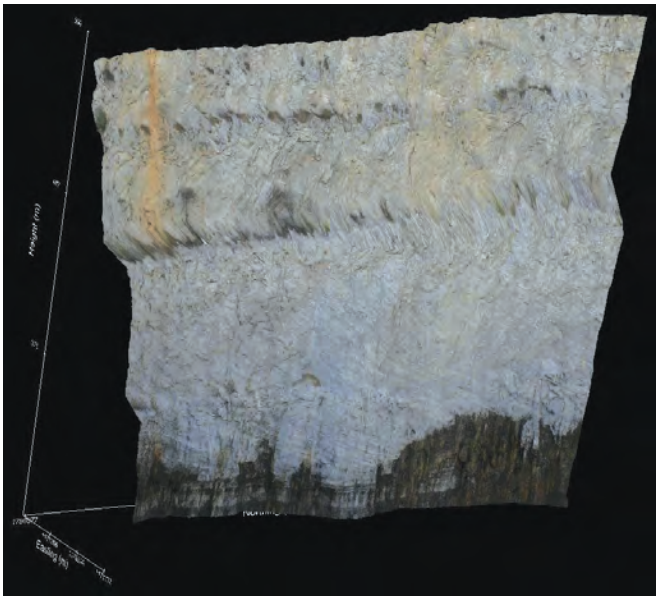

Figure A7.6 Three-dimensional stereomodel 3011-3012 with a draped orthophotograph (Figure A7.5) as viewed from the lower rear showing the prominent horizontal bench in the middle, and a smaller, less prominent bench in the lower left.

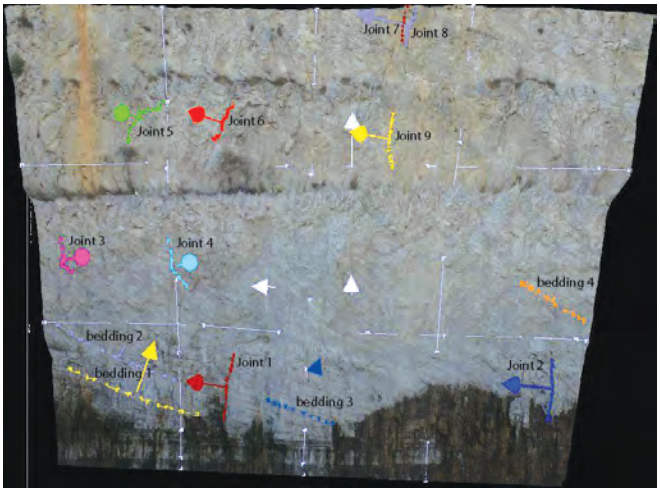

Figure A7.7 3-D image of stereomodel and annotated orthophotograph 3011-3012 showing joint traces and bedding planes digitized in Sirovision. Most joints are nearly vertical; however, a few joints are curved or oriented in other directions.

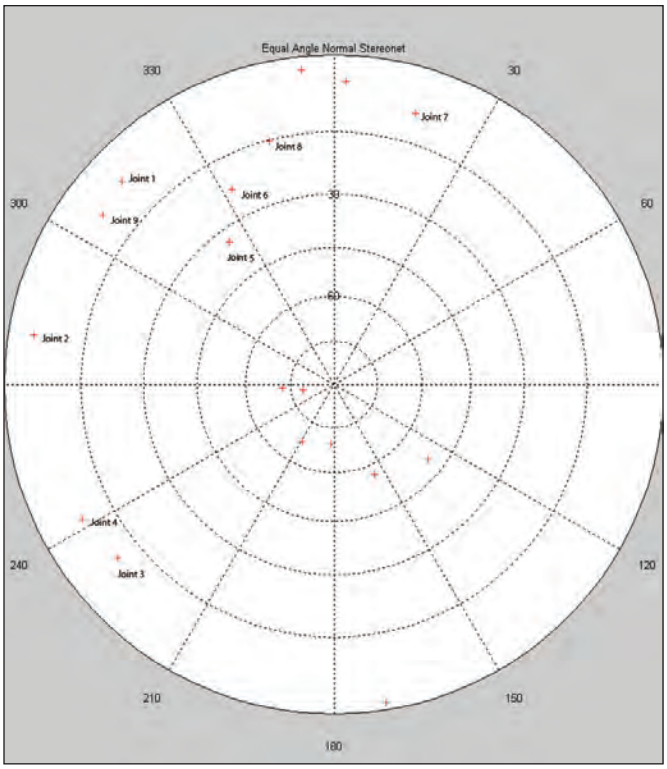

Figure A7.8 Stereonet showing dip magnitude and the direction of joints and bedding planes of stereomodel 3011-3012 listed in Table A7.1.

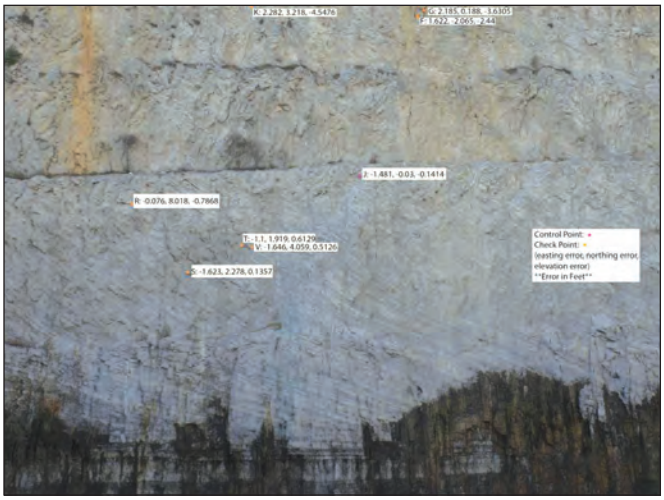

Figure A7.9 Control point J and check points for orthophotograph 3011-3012. Errors are shown in feet for easting, northing, and elevation.